Atmos. Chem. Phys. Discuss., https://doi.org/10.5194/acp-2017-947
Manuscript under review for journal Atmos. Chem. Phys.
Discussion started: 8 November 2017

Atmospheric Chemistry and Physics Discussions

Influence of Intense secondary aerosol formation and long range transport on aerosol chemistry and properties in the Seoul Metropolitan Area during spring time: Results from KORUS-AQ

Hwajin Kim[1,2] Qi Zhang[3,4*], and Jongbae Heo[5]

[1] Center for Environment, Health and Welfare Research, Korea Institute of Science and Technology, Seoul, Korea

[2] Department of Energy and Environmental Engineering, University of Science and Technology, Daejeon, Korea

[3] Department of Environmental Science and Engineering, Fudan University, Shanghai, China.

[4] Department of Environmental Toxicology, University of California, Davis, CA 95616, USA

[5] Center for Healthy Environment Education & Research, Graduate School of Public Health, Seoul National University, Seoul, Korea

*Corresponding author: Qi Zhang

Department of Environmental Toxicology, University of California 1 Shields Avenue, Davis, California 95616

Phone: (530)-752-5779

Email: dkwzhang@ucdavis.edu

Abstract

Non-refractory submicrometer particulate matter (NR-PM_1) was measured in the Seoul Metropolitan Area (SMA), Korea, using an Aerodyne high-resolution time-of-flight aerosol mass spectrometer (HR-ToF-AMS) from April 14 to June 15, 2016, as a part of the Korea-U.S. Air

Atmos. Chem. Phys. Discuss., https://doi.org/10.5194/acp-2017-947
Manuscript under review for journal Atmos. Chem. Phys.
Discussion started: 8 November 2017

Atmospheric Chemistry and Physics Discussions

Quality Study (KORUS-AQ) campaign. This was the first highly time-resolved, real-time measurement study of springtime aerosol in SMA and the results reveal valuable insights into the sources and atmospheric processes that contribute to PM pollution in this region.

The average concentration of submicrometer aerosol (PM_1 = NR-PM_1 + black carbon (BC)) was 22.1 μg m^{-3}, which was composed of 44% organics, 20% sulfate, 17% nitrate, 12 % ammonium, and 7 % BC. Organics had an average atomic oxygen-to-carbon (O/C) ratio of 0.49 and an average organic mass-to-carbon (OM/OC) ratio of 1.82. The concentration and composition of PM_1 varied dynamically due to the influences of different meteorological conditions, emission sources, and air mass origins. Four distinct sources of OA were identified via positive matrix factorization (PMF) analysis of the HR-ToF-AMS data: vehicle emissions represented by a hydrocarbon like OA factor (HOA; O/C = 0.15; 17% of OA mass), cooking activities represented by a cooking OA factor (COA; O/C = 0.19; 22% of OA mass), and secondary organic aerosol (SOA) represented by a semi-volatile oxygenated OA factor (SV-OOA; O/C = 0.44; 27% of OA mass) and a low volatility oxygenated OA factor (LV-OOA; O/C = 0.91; 34% of OA mass).

Our results indicate that air quality in SMA during KORUS-AQ was influenced strongly by secondary aerosol formation with sulfate, nitrate, ammonium, SV-OOA, and LV-OOA together accounting for 76% of the PM_1 mass. In particular, high temperature, elevated ozone concentrations, and photochemical reactions during daytime promoted the formation of SV-OOA, LV-OOA and sulfate whereas nocturnal processing of nitrogen oxides and daytime photochemical reactions promoted nitrate formation. In addition, gas-to-particle partitioning processes appeared to have enhanced nighttime SV-OOA and nitrate formation. During a period of 4 days (from May 20 to May 23), LV-OOA was significantly enhanced and accounted for up to 41% of the PM_1 mass. This intense LV-OOA formation event was associated with large enhancements of both anthropogenic and biogenic VOCs (e.g., isoprene, toluene), high concentration of O_x (= O_3 + NO_2), strong solar radiation, and stagnant conditions, suggesting that it was mainly driven by local photochemical formation. We have also investigated the formation and evolution mechanisms of severe haze episodes. Unlike the winter haze events which were mainly caused by intense local emissions coupled with stagnant meteorological conditions, the spring haze events appeared to be influenced by both regional and local factors. For example, there were episodes of long range transport of plumes followed by calm meteorology conditions, which promoted the formation and accumulation of local secondary species, leading to high concentrations of PM. Overall, our results

Atmos. Chem. Phys. Discuss., https://doi.org/10.5194/acp-2017-947
Manuscript under review for journal Atmos. Chem. Phys.
Discussion started: 8 November 2017

Atmospheric Chemistry and Physics Discussions

indicate that PM pollutants in urban Korea originate from complex emission sources and atmospheric processes and that the concentrations and composition of PM are controlled by various factors including meteorological conditions, local anthropogenic emissions, and upwind sources. Therefore, understanding the high aerosol pollution followed by efficient strategies to remove precursors are important to control the air pollution.

1 Introduction

Particulate matter (PM) in the atmosphere can reduce visibility, damage human health, and impact climate directly by absorbing and reflecting solar radiation and indirectly by modifying cloud formation and properties (IPCC, 2013;Pope III and Dockery, 2006;Pöschl, 2005). PM pollution in urban areas is commonly associated with elevated anthropogenic emissions, stagnant meteorological conditions, and regional transport of pollutants from upwind locations (Cao et al., 2012;Guo et al., 2014;Sun et al., 2014;Zheng et al., 2015;Molina, 2004;Young et al., 2015).

The Seoul Metropolitan Area (SMA) is one of the most populated and developed places in Korea and is ranked as the fourth largest metropolitan area in the world. SMA is experiencing persistent air quality problems despite of continuous regulatory control efforts for many years. Aerosol concentration in this area often exceeds the $PM_{2.5}$ annual standards set by the United States Environmental Protection Agency (US EPA, 12 μg m^{-3}) and the World Health Organization (WHO, 10 μg m^{-3}).

SMA is the commercial, industrial, and residential center of South Korea with a population of ~ 24 million. Air quality in SMA is driven predominantly by local anthropogenic emissions but is also influenced by emissions from surrounding areas such as industrial emissions in the west of SMA and emissions from biogenic, agricultural and biomass burning sources in the East (Kim et al., 2010). Air quality in SMA can also be influenced by long-range transport of air pollutants. For example, due to its location in the central-west of the Korean Peninsula facing the Yellow Sea on the west, air quality in SMA can be impacted heavily by continental outflows from mainland China (Kim et al., 2010). Furthermore, due to confluence of a wide range of emissions, ranging from local to regional, marine to continental, and biogenic to anthropogenic, the interactions among these emissions are likely as important as the emissions themselves in determining the formation and evolution of particulate pollutants in SMA. Consequently, developing effective mitigation strategy for air pollution in SMA remains a great challenge (Harrison and Yin, 2000).

Atmos. Chem. Phys. Discuss., https://doi.org/10.5194/acp-2017-947
Manuscript under review for journal Atmos. Chem. Phys.
Discussion started: 8 November 2017

Atmospheric Chemistry and Physics Discussions

In addition to various emission sources, previous studies have shown that the concentration and composition of ambient aerosol in SMA are influenced by atmospheric processes and meteorological conditions as well (Heo et al., 2009;Kim et al., 2017). For example, during winter, elevated anthropogenic emissions (e.g., from heating) coupled with a lower planetary boundary layer (PBL) height and stagnant meteorological conditions tend to be responsible for poor air quality in Seoul, although long-range transport of pollutants from upwind areas may have some influences as well (Kim et al., 2014;Kim et al., 2017). The severe air quality problem during spring in SMA is frequently driven by long range transport of wind-blown dust (yellow dust) and smokes from fires from the west and northwest (Kim et al., 2010). In addition, compared to winter, photochemical formation of secondary aerosol tends to be more intense due to elevated temperature and solar radiation during spring and affects air quality in SMA more actively. However, so far there is little information available on the formation, properties and transport of atmospheric aerosol during spring, although a fundamental understanding of aerosol chemistry and dynamics in SMA is necessary for predicting how changes in atmospheric composition influence air quality.

The Korea-U.S. Air Quality Study (KORUS-AQ) is an international cooperative air quality field study that took place in Korea in spring 2016. This field study was aimed at integrating information from satellites, aircraft and ground measurements, and model simulations to better understand satellite performance and atmospheric composition and to improve model fidelity in simulating the current atmospheric state and possible future scenarios (KORUS-AQ mission whitepaper: https://espo.nasa.gov/home/korus-aq). One of the key scientific goals of KORUS-AQ is to determine the most important factors governing ozone photochemistry and aerosol evolution. Specially, this study aims at addressing two questions for aerosol: 1) what portion of aerosol in SMA is comprised with secondary process and what are the major sources and factors to control its variation? and 2) How important are local and regional influences on air quality in SMA?

As part of the KORUS-AQ, many aerosol, gas-phase, and meteorological measurements were made at several ground sites in SMA during spring. One of the sites was located on the Korea Institute of Science and Technology (KIST) campus, where a comprehensive, real-time dataset on size-resolved chemical composition and number distribution of submicrometer particles (PM_1) was acquired – using an Aerodyne high-resolution time-of-flight aerosol mass spectrometer (HR-ToF-AMS) in parallel with a scanning mobility particle sizer (SMPS) for 2 months from April 14,

Atmos. Chem. Phys. Discuss., https://doi.org/10.5194/acp-2017-947
Manuscript under review for journal Atmos. Chem. Phys.
Discussion started: 8 November 2017

2016 to June 15, 2016. Here we report results from detailed analyses of this dataset. Specifically, in addition to the high-resolution mass spectra (HRMS) and elemental ratios determined by the HR-ToF-AMS, distinct organic aerosol (OA) factors were derived through analyzing HRMS to gain insights into the sources and atmospheric processing of OA. Our goals are to reach a detailed understanding of the chemical properties of aerosol particles in SMA and to elucidate the emission sources and formation and transformation processes that drive their temporal and diurnal variations over this region during spring. Given that SMA is located in a region impacted by both local emissions from anthropogenic and biogenic activities and long-range transported emissions from upwind sources, complex pollutant interactions tend to occur on fast time scales. An in-depth understanding of these processes will be useful for developing parameterization for future satellite retrievals, specifically for geostationary (GEO) satellites, which offer higher time and spatial resolution information compared to low Earth orbit (LEO), including detailed daily variation patterns of atmospheric pollutants.

Here, we report: (1) the mass concentrations, size distributions, chemical composition, and temporal and diurnal variations of PM_1 species; (2) the characteristics and dynamic variations of OA sources and processes using positive matrix factorization (PMF); (3) discussions on the intensive formation of secondary species; and (4) a case study of haze event.

2 Experimental Methods

2.1 Sampling site description

The KORUS-AQ field campaign took place in SMA from April 14 to June 15, 2016. A map of the SMA with the location of the ground-based sites is given in Fig. 1a. Measurements reported in this paper were performed on the 5th floor of a building on the campus of KIST (37.60N, 127.05E, 60 m above sea level) at ~ 7 km to the northwest of the Olympic Park, which is the main supersite of KORUS-AQ. Detailed descriptions of the KIST site can be found in Kim et al. (2017). Briefly, KIST is located ~ 400 m from a busy highway and is surrounded by a residential area and a commercial area, thus the air quality at this site tends to be influenced by abundant anthropogenic and primary sources. During spring, KIST, SMA in general, is influenced by highly consistent winds from west and south west (Fig. 1 c, d), where a number of cities and large-scale industrial facilities are located (Fig. 1a) and are significant sources of NO_x and SO_x (Kim et al., 2017).

Atmos. Chem. Phys. Discuss., https://doi.org/10.5194/acp-2017-947
Manuscript under review for journal Atmos. Chem. Phys.
Discussion started: 8 November 2017

However, sometimes, dominant wind was blown from north and east, where emissions from agricultural and biogenic sources are generally more intense (Fig. S1).

2.2 Measurements

At the KIST site (37.60N, 127.05E), NR-PM_1 components including sulfate, nitrate, ammonium, chloride, and organics as well as their size distributions were measured by an Aerodyne HR-ToF-AMS (DeCarlo et al., 2006) at a time resolution of 3 min. In parallel, black carbon (BC) concentration was measured every minute with a multi angle absorption photometer (MAAP; Thermo Fisher Scientific, Waltham, MA, USA). Both instruments sampled downstream of a $PM_{2.5}$ cyclone (URG Corp.; Chapel Hill, NC, USA) and Nafion dryer (Perma Pure LLC, USA). The number size distributions of aerosol particles with mobility diameters between 20–1000 nm were measured by a scanning mobility particle sizer (SMPS 3080; TSI Inc., St Paul, MN, USA). The concentrations of trace gases (e.g., CO, O_3, NO_2 and SO_2) were acquired at the Gireum site (37.61N, 127.03E) operated by the Seoul Research Institute of Public Health and Environment (http://www.airkorea.or.kr). Meteorological measurement data such as ambient temperature, relative humidity (RH), wind speed and wind direction were obtained from the nearby Jungreung site (37.61N, 127.00E) maintained by the Korea meteorological administration (http://www.kma.go.kr). VOC data were obtained from the Gwangjin supersite (37.55N, 127.09E) maintained by the Seoul Research Institute of Public Health and Environment ((https://health.seoul.go.kr). The data reported in this paper are in local time, which is Korea Standard Time (KST) and is 9 h earlier than the Universal Coordinated Time (UTC).

In this study, the HR-ToF-AMS was operated in the standard configuration and obtained mass spectra (MS) and particle time of flight (PToF) data. Furthermore, the HR-ToF-AMS was operated under the 'V' and 'W' modes, where high sensitivity but low mass resolution was achieved in 'V' mode, and low sensitivity, but high mass resolution was achieved in 'W' mode. Ionization efficiency (IE) and particle sizing calibrations were performed following standard protocols (Canagaratna et al., 2007) immediately before, during, and at the end of the measurement period.

2.3 AMS data analysis

2.3.1 Basic HR-ToF-AMS data analysis

HR-ToF-AMS data were processed and analyzed using the standard toolkit (SeQUential Igor data RetRiEval (SQUIRREL; ver. 1.57I), and PIKA (ver. 1.16I; available for download at

http://cires.colorado.edu/jimenez-group/ToFAMSResources/ToFSoftware/index.html)) within Igor Pro (Wavemetrics, Lake Oswego, OR, USA). Details on the data processing procedures are described in previous papers (e.g., Aiken et al., 2008;Allan et al., 2004;Jimenez et al., 2003;Setyan et al., 2012). Briefly, the standard fragmentation table described by Allan et al. (2004) was used, with some modifications, to process the raw MS. The modifications were based on data from six measurements of filtered ambient air to properly remove the background contributions from gas-phase signals to particle measurements. Specifically, adjustments were made to the measured CO_2^+ (m/z = 44) signal to remove the contributions from gas phase CO_2 as well as the $^{16}O^+$ to $^{14}N^+$ ratio for air signals at m/z = 29 based on measurements of particle-free ambient air. Relative ionization efficiencies (RIE) of 1.1, 1.07, and 3.938 were used for nitrate, sulfate, and ammonium, respectively, based on values determined from calibrations using pure NH_4NO_3 and $(NH_4)_2SO_4$ particles. A composition-dependent collection efficiency (CDCE) was applied to the data based on an algorithm by Middlebrook et al. (2012). The campaign average (± 1σ) CDCE was 0.5 ± 0.01(Fig. S2).

The quantification of NR-PM_1 species was validated through comparisons between the total PM_1 mass (PM_1 = NR-PM_1 + BC) and the apparent particle volume measured by the SMPS (Fig. S3). As shown in Fig. S3c, the SMPS-measured particle volume correlated strongly with the AMS measured total mass (R^2 = 0.88). The slope from the linear fit of PM_1 mass against SMPS volume is 1.24 g/cm^3, which was lower than the average (± 1σ) particle density of 1.50 (± 0.08) g/cm^3 estimated using the measured chemical composition in this study (Zhang et al., 2005b) (Fig. S3d). Note that the average (± 1σ) organic aerosol density was estimated to be 1.21 (± 0.07) g/cm^3 based on the approach reported in Kuwata et al. (2012) using the average elemental ratios of bulk OA determined using the Aiken-Ambient method (Aiken et al., 2008) (Table S1, Fig. S4). The evolution pattern of the AMS total mass-based size distribution also compared well with the volume-based size distribution from SMPS measurements throughout the day (Fig. 6a and b). The detection limits of the main chemical components by the HR-ToF-AMS are listed in Table 1, and are generally far lower than the observed concentrations. All the reported mass concentrations in this study are based on ambient conditions.

The elemental ratios between oxygen, carbon, hydrogen, nitrogen and sulfur as well as the organic mass to carbon ratio (OM/OC) of OA, were determined by analyzing the W mode high resolution mass spectra (HRMS) data using both the Aiken-Ambient method (Aiken et al., 2008)

Atmos. Chem. Phys. Discuss., https://doi.org/10.5194/acp-2017-947
Manuscript under review for journal Atmos. Chem. Phys.
Discussion started: 8 November 2017

and the updated method recently reported by Canagaratna et al. (2015). The ratios reported by the two methods correlate very well and the Canagaratna method report higher values by a factor of 1.28, 1.02 and 1.28 for O/C, H/C and OM/OC, respectively (Table S1 and Fig. S4). Unless otherwise indicated, the O/C, H/C, and OM/OC ratios reported in this paper are all from the Canagaratna et al. (2015) method.

2.3.2 Positive Matrix Factorization (PMF) of the HR-ToF-AMS Mass Spectra

The HRMS acquired during this study were analyzed using PMF. The analysis was performed using the PMF2 algorithm in robust mode (Paatero and Tapper, 1994), with the PMF Evaluation Toolkit (PET ver 2.05) (Ulbrich et al., 2009) downloaded from http://cires1.colorado.edu/jimenez-group/wiki/index.php/PMF-AMS_Analysis_Guide#PMF_Evaluation_Tool_Software. The data and error matrices were prepared according to the protocol described by Ulbrich et al. (2009) and outlined in Table 1 of Zhang et al. (2011).

The PMF analysis was performed on the combined matrices of organic and inorganic ions using the method reported in Sun et al. (2012) since including the inorganic signals allows better separation and evaluation of physically meaningful organic aerosol factors. For example, the solutions of the combined matrix provide information on the distributions of inorganic signals among different sources and the association between inorganic and organic aerosol components in individual factors. This information is helpful for interpreting the sources, chemical characteristics, and evolution processes of different types of OA (Sun et al., 2012;Zhou et al., 2017).

The combined matrix includes organic ions in the range of m/z = 12 to 120 amu and the major ions of inorganic species, i.e., SO^+, SO_2^+, HSO_2^+, SO_3^+, HSO_3^+, and $H_2SO_4^+$ for sulfate; NO^+ and NO_2^+ for nitrate; and NH^+, NH_2^+, and NH_3^+ for ammonium. Chloride related ions were not included because of their low signal-to-noise ratios during this study. The ion signals in the HRMS and error matrices analyzed with PMF were expressed in nitrate-equivalent concentrations. The number of factors (p) in the solution was explored from one up to nine with varying rotational parameters ($-1 \leq$ FPEAK ≤ 1, in increments of 0.1). After a detailed evaluation of the key diagnostics, i.e., mass spectral signatures, diurnal profiles, and correlations with external tracers, as outlined in Zhang et al. (2011), the six factor solution (four organic factors and two inorganic factors) with fPeak = 0, was selected for further analyses. A summary of the key diagnostics is presented in Fig. S5 in the Supplement. The six factor solution was found to be very stable as the

Atmos. Chem. Phys. Discuss., https://doi.org/10.5194/acp-2017-947
Manuscript under review for journal Atmos. Chem. Phys.
Discussion started: 8 November 2017

mass distributions of the factors remained relatively constant between fPeaks -0.7 and +0.7 (Fig. S5c). Fig. S6 shows the mass spectra and the time series of the five- and seven-factor solutions. The five-factor solution was unable to deconvolve a meaningful COA factor whereas the temporal variations of the organic factors from the seven-factor solution showed indications of factor splitting and mixing of inorganics. For example, two separate nitrate and sulfate factors (factors 1 and 2) as well as one mixed factor of nitrate and sulfate (factor 3) were identified. Given the fact that having only two inorganic factors (i.e., the 6-factor solution set) did not influence the separation of the other organic factors, it was not necessary to go for higher number of factors. Consequently, the 6-factor solution, which resolved HOA, COA, two types of OOA and two inorganics was chosen as it appears to best represent OA sources and processes in the SMA during KORUS-AQ.

In this study, we also performed regular PMF analysis on the OA matrix only (Ulbrich et al., 2009), but the analysis was unsuccessful at retrieving meaningful factors (Fig. S7). A minimum of four factors was needed to adequately account for the observed variance but the solution showed indications of mixing factors without being able to resolve a meaningful HOA factor. One the other hand, the five-factor solution, although was able to resolve two POA factors representing COA and HOA, respectively, it showed indications of splitting and mixing of OOA factors (Fig. S7).

2.3.3 Backtrajectory and Bivariate conditional probability function analyses

In this study, 96-h backtrajectories were calculated every hour using version 4.9 of the Hybrid Single-Particle Lagrangian Integrated Trajectory (HYSPLIT) model (Draxler, 2012;Draxler, 1997) for the sampling periods from April 14, 2016 to June 15, 2016. Every trajectory was released at half of the mixing height at the KIST (latitude: 37.60N; longitude: 127.05E) and the average starting height for the back trajectories for entire period of this study was approximately 190 m (Fig. S8). Note that the half of mixing height was automatically calculated by the HYSPLIT model. To identify pollutant characteristics in different predominant transport patterns, cluster analysis was performed on the trajectories using HYSPLIT4 and 5 clusters were identified according to their similarity in spatial distribution. In addition, backtrajectories were calculated separately for episode periods, i.e., organic dominant period (from May 20 to May 24) and Haze period (from May 26 to May 31) to identify the directions and characteristics of significantly influenced plumes during those periods.

Atmos. Chem. Phys. Discuss., https://doi.org/10.5194/acp-2017-947
Manuscript under review for journal Atmos. Chem. Phys.
Discussion started: 8 November 2017

In addition, conditional probability function (CPF) (Kim et al., 2003) was performed to estimate the local sources and their impacts on PM_1 composition and individual organic aerosol sources from PMF analysis, using wind directions coupled with the time series of concentration of each species. The CPF plots represent the probability that a specific compound or source is located in certain wind direction, assisting to find local point sources.

3 Results and discussions

3.1 Overview of submicron aerosol characteristics

3.1.1 Temporal variations of PM_1 composition and chemical properties

The overall characteristics and temporal variations of PM_1 at KIST during KORUS-AQ are shown in Fig. 2, along with the time series of gaseous pollutants, e.g., CO, SO_2, O_3, and O_x (O_x = O_3 + NO_2; (Herndon et al., 2008)), and meteorological conditions (RH, temperature, wind direction, wind speed). From April 14, 2016 to June 15, 2016, the average concentration of PM_1 (= NR-PM_1 + BC) was 22.1 μg m^{-3}, ranging from 0.76 to 71 μg m^{-3}. In addition to a severe haze episode with daily PM_1 concentration above 30 μg m^{-3} that continued for 6 days during May 26- May 31, shorter haze episodes (daily PM_1 > 30 μg m^{-3}) occurred several times as well (Fig. 2). In between high loading periods, aerosol concentration was relatively low with daily PM_1 concentration typically lower than 14 μg m^{-3}. The dramatic variations in PM_1 mass concentrations (0.76 to 71 μg m^{-3} for 2.5 min average; Fig. 2f) and other pollutants (Figs. 2c, d), such as CO (0.2 to 1 ppm for 1min average), O_3 (3 to 82 ppb for 1min average), and NO_2 (6 to 76 ppb for 1min average) reflect the impacts of dynamic changes in emission sources, atmospheric processes, and meteorological conditions on air quality in SMA during spring.

As indicated in Figs. 2g and h, the variations of individual PM_1 components were also substantial. For instance, the mass concentration of organics ranged from 0.39 to 39 μg m^{-3} during this study and on May 20, it rapidly increased from 7.6 μg m^{-3} to 24 μg m^{-3} over a period of ~ 25 minutes and reached as high as 39 μg m^{-3} on May 23 (Fig. 2h). The accumulation of OA during this episode appeared to be related to a large enhancement of VOCs (e.g., isoprene, toluene) (Fig. 2e) coupled with high concentration of O_x (O_3 + NO_2), strong solar radiation and stagnant conditions, which together promoted intensive formation of secondary organic aerosol (SOA). The mass concentration of sulfate also varied widely from 0.19 to 21 μg m^{-3} during the entire period and increased from 1.2 μg m^{-3} to 20 μg m^{-3} from May 24 to May 26, likely due to favorable

Atmos. Chem. Phys. Discuss., https://doi.org/10.5194/acp-2017-947
Manuscript under review for journal Atmos. Chem. Phys.
Discussion started: 8 November 2017

meteorological conditions for sulfate formation and influences from long range transport. Investigation of these different events (e.g., haze periods, high organic/or sulfate period) can provide insights into how different sources and atmospheric processes influence air quality in this region. The variation of nitrate concentration was substantial too, from 0.05 μg m^{-3} to 23.4 μg m^{-3} with low concentrations generally occurring during daytime due to high temperature and low humidity. Detailed discussions on the processes that led to high aerosol pollution events are presented in section 3.4 and 3.5.

Since the molar equivalent ratios of total inorganic anions to cation for NR-PM_1 (= (SO_4^{2-}/48 + NO_3^-/62 + Cl^-/35.5) / (NH_4^+/18)) were close to 1 (Fig. S9), submicron aerosols appeared to be mostly neutralized and the ionic species were mainly present in the forms of NH_4NO_3, $(NH_4)_2SO_4$, and NH_4Cl. Possible sources of ammonium in the SMA include on-road vehicle emissions, neutralizer usage in industry, and agricultural emissions at the outskirt of SMA.

Overall, organics were an important aerosol component, on average accounting for 44% of PM_1 mass. POA (= HOA + COA) and SOA (= SV-OOA + LV-OOA) accounted for 59% and 41%, respectively, of the OA mass (detailed discussions on OA sources are provided in section 3.3). Secondary inorganic aerosol (SIA = sulfate + nitrate + ammonium) on average accounted for 37 % of the total PM_1 mass with sulfate contributing the most (20%) (Fig. 1e). The non-refractory chloride concentrations measured by the HR-ToF-AMS were mostly below detection limit during the present study. On average, ~ 24% of PM_1 was composed of primary materials (POA + BC), with the remainder (76%) being secondary species (NO_3^- + SO_4^{2-} + NH_4^+ + SOA) (Fig.1e), indicating that the aerosol pollution problem in SMA during spring is mainly caused by secondary aerosol formation.

The average concentration and composition of PM_1 measured in SMA during this study were significantly different from those measured during wintertime. For instance, compared to winter, the average PM_1 concentration was lower during spring (22 vs 27 μg m^{-3}), the mass fraction of sulfate was higher (20 vs 10%) but that of nitrate was lower (17 vs 24 %) (Kim et al., 2017), and the total contribution of secondary species was higher (76 vs 64%). As discussed in following sections, these differences reflect the differences between the two seasons in meteorological conditions and emissions and formation processes of air pollutants.

Atmos. Chem. Phys. Discuss., https://doi.org/10.5194/acp-2017-947
Manuscript under review for journal Atmos. Chem. Phys.
Discussion started: 8 November 2017

Atmospheric Chemistry and Physics Discussions

3.1.2 Diurnal patterns of PM_1 composition and formation processes

As shown in Fig. 3, the diurnal cycles were vastly different among different aerosol species. The daily variation of the average concentration of sulfate was relatively flat and its mass-based size distribution shows a persistent accumulation mode that peaks at 650 nm (D_{va}) (Fig. S10). These observations together with a dispersed feature of the sulfate bivariate polar plot (Fig. S12) indicate that particulate sulfate over SMA is mainly associated with regional sources, such as the industrial facilities located on the west and southwest of SMA (Fig. 1) (Kim et al., 2017). Indeed, the polar plot of SO_2 shows a strong association of high SO_2 concentrations with west and southwest winds (Fig. S12). Figs. 4c shows the diurnal patterns of springtime sulfate, SO_2, and the molar ratio of sulfate (SO_4^{2-}) to SO_x (= SO_4^{2-} + SO_2), i.e., f_{SO4}, which is an indicator for the extent of SO_2 oxidation (Kaneyasu et al., 1995)). f_{SO4} decreased from 0.24 to 0.21 between 6:00 - 10:00, during which SO_2 increased by ~ 1 ppb (Fig. 4a). This change was likely due to the breaking of the boundary layer which mixed down air masses more enriched of SO_2 from aloft. Also, f_{SO4} increased gradually from 11:00 till 6:00 of the next day, which can be explained by daytime photochemical formation of H_2SO_4 from SO_2 + OH (Fig. 4c) and aqueous phase oxidation of SO_2 facilitated by the high RH condition at night. Indeed, SO_2 began to decrease at ~ 19:00, when RH increased and T decreased (Fig. 4a). Similar trends were observed during winter as well, although higher SO_2 and lower SO_4 and fSO_4 were observed (Fig. 4d). Lower SO_2 concentration during spring was likely due to less coal combustion for heating and the higher SO_4 and fSO_4 were due to more efficient conversion of SO_2 to SO_4 during spring under stronger solar radiation or more regional transport of SO_4. Previous study indicates that nighttime aqueous phase processing was an important driver for sulfate formation during winter in SMA (Kim et al., 2017). However, aqueous phase sulfate production appeared to be less important than gas phase photochemical oxidation of SO_2 and regional transport during spring. Indeed, fSO_4 correlated less well with RH during spring than during winter (R^2 = 0.27 vs. 0.59) (Fig. S13).

Unlike sulfate, nitrate shows more dynamic diurnal cycles during both spring and winter. Overall, nitrate concentration was lower in spring than in winter despite faster photochemical production. This is due to higher temperature (Figs. 4a,b), which drives the evaporation of ammonium nitrate, particularly during spring daytime. Indeed, a depression of nitrate concentration occurred during the daytime of spring, whereas a midday peak (between 9:00-15:00) due to photochemical formation of nitrate was observed during winter. The overnight increase of

Atmos. Chem. Phys. Discuss., https://doi.org/10.5194/acp-2017-947
Manuscript under review for journal Atmos. Chem. Phys.
Discussion started: 8 November 2017

Atmospheric Chemistry and Physics Discussions

nitrate during springtime was likely driven by enhanced gas-to-particle partitioning of ammonium nitrate associated with lower temperature as well as nighttime formation of nitrate (e.g., through N_2O_5 hydrolysis), which is consistent with the high concentrations of O_3 (~20.0 ppb) and NO_2 (~41.7 ppb) throughout the night (18:00 – 6:00). However, the peak nitrate concentration (at ~9:00) occurred 3h later than the peaking of the ammonium nitrate equilibrium constant (K_{AN}) (~6:00), which might be due to the mixing down of a nocturnal residual layer (Prabhakar et al., 2017). Significant nitrate formation through nighttime chemistry occurred during winter as well, due to lower temperature and relatively high nighttime concentrations of NO_2 and O_3. However, nighttime nitrate formation was less important in winter compared to spring as the product of NO_2 and O_3 ($[NO_2][O_3]$) – an indicator for nighttime formation of HNO_3 and particulate nitrate (Young et al., 2016) – was on average more than a factor of 2 lower (Figs. 4a,b). Therefore, the elevated nighttime nitrate concentration in winter was primarily due to enhanced gas-to-particle partitioning and formation of NH_4NO_3.

Organics dominated PM_1 composition throughout the day, with 1-hr average mass fractions varying from 40 to 48% (Fig. 3). The average diurnal profile of organics showed elevated concentration overnight and a clear daytime peak from 13:00 to 18:00. The nighttime enhancement was consistent with the accumulation of primary emissions from traffic and cooking due to low boundary layer height and stagnant air condition whereas the daytime enhancement was likely the outcome of photochemical formation of SOA. Detailed discussions are given in Section 3.3.

BC presented two peaks, one occurring during morning rush hour (7:00 – 10:00) and the other in the afternoon between 14:00 – 15:00 (Fig. 3). Similar trends were observed with HOA (section 3.3.2) and particle number concentration (Fig. 3), indicating that both peaks of BC were contributed by vehicle emissions. The morning rush hour peak of primary air pollutants is commonly observed in many other studies as well as during winter at the same site (Kim et al., 2017), however, the enhancement of these species in the afternoon, when elevated mixed layer height tends to dilute primary pollutants, is unique. In addition, the afternoon increase of BC, HOA, and particle number concentration, began at ~12:00 and reached a maximum around 16:00 (Fig. 3). This time period corresponded to the effective transport of air masses from urban and industrial areas located on the south and southwest of the KIST site (Fig. 1a) by a predominant southwesterly flow during 11:00 – 17:00 (Fig. S1). With an average wind speed of ~ 2 m/s, the southwesterly wind would take ~ 1 – 5 hours to bring plumes from upwind urban sites that are ~

Atmos. Chem. Phys. Discuss., https://doi.org/10.5194/acp-2017-947
Manuscript under review for journal Atmos. Chem. Phys.
Discussion started: 8 November 2017

7.2 km (e.g., Anyang) to 36 km (e.g., Incheon, Siheung and Ansan) away from the KIST site (Fig. 1). Furthermore, the large increase of particle number concentration (Fig. 3) and the apparent growth of ultrafine particles (Fig. 6c) between ~12:00 and 16:00 suggest that new particle events might have happened in association with transport of plumes from southwest.

3.2 Size distributions of the main components of PM_1

Fig. 5 shows the average mass-based size distributions of NR-PM_1 species over the entire KORUS-AQ campaign and their daily evolution behaviors. Sulfate, nitrate and ammonium in spring all show very similar size distribution profiles with a mode peaking at around 650 nm in vacuum aerodynamic diameter (D_{va};(DeCarlo et al., 2004)) (Fig. S10), suggesting that SIA were internally mixed. The springtime size distribution profiles of SIA at KIST are somewhat different than those observed during winter, which peaked around 400-500 nm (Kim et al., 2017). The finding of bigger particle sizes during spring than in winter could be due to faster particle growth rates caused by higher photochemical activity during spring. Similarly, a recent study in Beijing reported that the peak size of SIA during summer (600 nm in D_{va}) was bigger than during winter (350 nm) (Hu et al., 2016).

The average mass-based size distribution of organics was in general wider than those of inorganic species with a peak at ~ 550 nm and a shoulder peaking at ~ 300 nm and extending down to ~ 60 nm (Fig. 5b). Similar observations were made in the winter at SMA and a number of urban areas in China and North America (e.g., (Kim et al., 2017) and references in therein). The wider size distribution of organics reflected the contributions made by both primary and secondary aerosols, i.e., the ultrafine mode dominated by primary aerosols and the accumulation mode comprised mainly of secondary aerosols. The mode of the organics in spring (500–600 nm) was bigger than in winter (400 nm), likely due to the same reason that the size mode of SIA was bigger during spring – enhanced photochemical activity for secondary aerosol formation in spring than in winter as well as less contributions of primary particles to fine mode particles from vehicular, cooking, and biomass burning sources. The average size distribution of organic was relatively constant throughout the day but there were changes in the mass concentration of accumulation mode organics during daytime (12:00-16:00) and nighttime (20:00-24:00) (Fig. S11). The daytime enhancement might be due to the photochemical formation of SOA whereas the nighttime enhancement was possibly caused by accumulation of aged POA as well as semi-volatile SOA (SV-OOA, section 3.3.2.3) due to lower PBL (section 3.3.2.1).

Atmos. Chem. Phys. Discuss., https://doi.org/10.5194/acp-2017-947
Manuscript under review for journal Atmos. Chem. Phys.
Discussion started: 8 November 2017

The organic fraction was above 50% across the whole size range and almost 100% in ultrafine mode particles (especially in D_{va} < 100nm), whereas SIA dominated (> 60% of NR-PM_1) in accumulation mode particles with D_{va} > 500 nm in spring (Fig. 5).

3.3 Characteristics and source apportionment of organic aerosol

3.3.1 Bulk composition and elemental ratios of OA

Atmospheric OA are composed of complex materials that originate from different sources and have undergone different atmospheric processes. Understanding the chemical composition and sources of OA is important for estimating the environmental and health impacts of aerosols and designing efficient mitigation strategies. Overall, OA from SMA during spring was found to be composed of approximately 66% carbon, 25% oxygen, 8% hydrogen, and 2% nitrogen (Fig. 7). The average carbon-normalized molecular formula of OA was $C_1H_{1.67}O_{0.49}N_{0.02}S_{0.002}$, yielding an average organic mass-to-carbon ratio (OM/OC) of 1.82. The average elemental ratios, which were calculated using the updated elemental analysis method (Canagaratna et al., 2015), are within the range of the revised values observed at other urban locations (Canagaratna et al., 2015;Young et al., 2016 and references therein). The largest component of the OA mass spectral signal was the $C_xH_y^+$ ions (57%, Fig. 7), followed by $C_xH_yO_1^+$ (25%) and $C_xH_yO_2^+$ (11%), with smaller contributions from the $C_xH_yN_p^+$ (4%), and $C_xH_yN_pO_z^+$ (2%). The largest peak in the average OA spectrum was at *m/z* = 44 (8.9% of the total OA signal; Fig. 7a) and it was composed of 87% CO_2^+, 4.7% $C_2H_4O^+$, 3.3% CH_2NO^+, 2.3 % $C_2H_6N^+$, and 0.2% $C_3H_8^+$. The second largest peak (8.3% of the total OA signal) in the average OA spectrum was at *m/z* = 43, which was dominated by the $C_2H_3O^+$ (70.6%), $C_3H_7^+$ (26.5%), $C_2H_5N^+$ (1.6%), and $CHON^+$ (0.7%). The peak at *m/z* = 57, which has been used as a tracer for hydrocarbon like organics from vehicle emissions accounted for 2.2% of the total OA signal, and was composed predominantly of $C_4H_9^+$ (64%) and $C_3H_5O^+$ (33%) in this study.

Upon examining the diurnal patterns of the atomic ratios among elements in OA, we found that the pattern of O/C and OM/OC ratios are similar but different from H/C, due to variations in the relative contributions of POA and SOA. Although organic ions containing nitrogen had relatively low abundance (average N/C = 0.02), nitrogen-to-carbon (N/C) ratios showed distinct diurnal profiles with a bimodal feature peaking at 10:00 and 16:00, respectively. The similarities between the N/C and O/C diurnal profiles suggest that particulate organic nitrogen (PON)

Atmos. Chem. Phys. Discuss., https://doi.org/10.5194/acp-2017-947
Manuscript under review for journal Atmos. Chem. Phys.
Discussion started: 8 November 2017

compounds in SMA during spring were strongly influenced by secondary processes. Indeed, as discussed in section 3.3.2.3 and shown in Fig. S14, nitrogen containing organic ions correlated well with both SV-OOA and LV-OOA factors but poorly with POA factors.

3.3.2 Organic aerosol source apportionment and characteristics of OA factors

Separation of distinct OA sources can be achieved through the application of multivariate models, such as PMF (Lanz et al., 2007;Ulbrich et al., 2009;Zhang et al., 2011). In this study, four distinct OA factors were determined, including two types of POA (HOA and COA) and two types of OOA (LV-OOA and SV-OOA). The O/C ratios for LV-OOA, SV-OOA, COA, and HOA were 0.91, 0.44, 0.19 and 0.15, respectively. The elemental ratios of the factors were estimated using the method reported by Canagaratna et al. (2015). A comparison with the O/C and H/C ratios determined by the method of Aiken et al. (2008) can be found in Table S1 and Fig. S4.

An overview of the chemical composition and temporal variations of the four OA factors are shown in Fig. 1i and Fig. 8. LV-OOA (34%) represents the largest fraction of the OA mass followed by SV-OOA (27%), COA (22%) and HOA (17%). Together, SOA on average accounted for 61% of the total OA mass and POA accounted for 39 % (Fig. S16). The chemical composition and temporal variations of each factor are discussed in detail below.

3.3.2.1 Hydrocarbon-like OA (HOA)

Alkyl fragments ($C_nH_{2n+1}^+$ and $C_nH_{2n-1}^+$) made a substantial contribution to the HOA spectrum, with major peaks at *m/z*'s 41, 43, 55, and 57 which were mostly composed of $C_3H_5^+$, $C_3H_7^+$, $C_4H_7^+$, and $C_4H_9^+$ ions, respectively (Fig. 8a). These major peaks and the overall picket fence fragmentation pattern resulting from the $C_nH_{2n+1}^+$ ions are typical features of the HOA spectra reported in other studies and are due to the association of these aerosols with fossil fuel combustion (e.g.,Alfarra et al., 2007;Lanz et al., 2008;Sun et al., 2011b;Zhang et al., 2005a;Huang et al., 2010;Morgan et al., 2010;Ng et al., 2011;Collier, 2015;Ge et al., 2012a;Kim et al., 2017;Young et al., 2016). In addition, strong correlations were observed between the time series of HOA and the $C_nH_{2n+1}^+$ and $C_nH_{2n-1}^+$ ions, e.g., $C_3H_7^+$ (r = 0.87), $C_4H_7^+$ (r = 0.81), $C_4H_9^+$ (r = 0.95), and $C_5H_{11}^+$ (r = 0.96) (Fig. S17 and Table 2). Due to the dominance of chemically reduced hydrocarbon species, the O/C ratio of the HOA was low (0.15), whereas the H/C ratio was high (2.00).

Atmos. Chem. Phys. Discuss., https://doi.org/10.5194/acp-2017-947
Manuscript under review for journal Atmos. Chem. Phys.
Discussion started: 8 November 2017

Two peaks in the diurnal pattern of HOA were observed, occurring in morning rush hour and afternoon, respectively. As discussed in Sections 2.1.2 and 2.3.1, similar diurnal pattern was observed with BC and particle number which are indicators of primary emission. Possible reasons for the afternoon peak are the influences of transportation of traffic plumes emitted at urban areas located to the southwest of SMA. The transportation possibly occurred due to active atmospheric circulation together with a change of wind direction to predominantly southwest at ~11:00. The distinct differences between weekday- and weekend-patterns for BC and HOA (Fig. 3), i.e., substantially reduced morning rush-hour and afternoon peaks over the weekend, further support this explanation. The morning peaks in HOA and BC during weekends might be influenced by the highway next to the sampling site, where heavy traffic tended to occur during weekend morning as residents drive out of SMA. A similar weekend effect on primary aerosol components was observed in SMA during winter (Kim et al., 2017) and in urban and suburban sites in the U.S. as well (Young et al., 2016;Zhou et al., 2016).

As shown in Fig. 8e, a slow increase of HOA concentration began at ~16:00 and persisted till the next morning, suggesting that the shallow PBL enhanced the gradual accumulation of the pollutants from vehicle emissions. The average ratio of HOA/BC was 1.03 which is lower than the value from light-duty vehicles (1.4) and higher than that from diesel trucks emission (0.5) (Ban-Weiss et al., 2008), suggesting that SMA is influenced by mixed traffic emission of both gasoline and diesel vehicles. Similar HOA/BC values were observed in other large urban areas, such as Pittsburgh (1.41 ± 0.22; (Zhang et al., 2005c)), New York City (1.29) (Sun et al., 2011b), Mexico City (1.25) (Aiken et al., 2009), and Xianghe, China (0.91) (Sun et al., 2016). The ratio was lower in winter in Korea (0.58), probably due to the impacts of biomass burning during winter (Kim et al., 2017).

On average, HOA contributed 17% of the total OA, which was similar to the number observed in winter (16 %) (Kim et al., 2017).

3.3.2.2 Cooking OA (COA)

COA has been widely reported in urban areas with high population densities (e.g., He et al., 2010;Huang et al., 2010;Mohr et al., 2012;Sun et al., 2011b;Young et al., 2016;Ge et al., 2012a;Wang et al., 2016b;Xu et al., 2014;Hayes et al., 2013). In this study, COA was found to account for 22% of the total OA mass, higher than HOA (Fig. S16). The diurnal pattern of COA displayed a large evening peak at ~ 19:00, i.e., dinner time, and a small lunch time peak at ~ 12:00.

Atmos. Chem. Phys. Discuss., https://doi.org/10.5194/acp-2017-947
Manuscript under review for journal Atmos. Chem. Phys.
Discussion started: 8 November 2017

Atmospheric Chemistry and Physics Discussions

Elevated COA concentration and larger fractional contribution to OA mass were observed throughout the night (Figs. 3 and 8f).

Similar to HOA, the mass spectrum of COA contained many alkyl fragments, but to a lesser extent (71.9 % of the total signal in COA spectrum compared to 81.5 % of the total signal in HOA spectrum) (Fig. S16). COA also contained significantly larger amounts of oxygen containing ions than HOA (e.g., $C_xH_yO_1^+$ = 21.0% vs. 11.5% and $C_xH_yO_2^+$ = 5.2% vs. 4.9%) (Fig. S16), and thus had a higher O/C ratio (0.19 vs 0.15) and a lower H/C ratio (1.83 vs. 2.00). The O/C ratio (0.19) of COA in spring was found to be higher than that in winter (0.14) but both values were within the range of the O/C ratios of COA observed in other studies (e.g., Barcelona (0.27) (Mohr et al., 2012), New York City (NYC) (0.23) (Sun et al., 2011a) and Fresno (0.14 in 2010 (Ge et al., 2012b) and 0.19 in 2013 (Young et al., 2016)). Key tracers for identifying the presence of aerosols from cooking related activities, such as $C_3H_3O^+$ (*m/z* 55), $C_3H_5O^+$ (*m/z* 57), $C_5H_8O^+$ (*m/z* 84) and $C_6H_{10}O^+$ (*m/z* 98) (He et al., 2004;Adhikary et al., 2010;Mohr et al., 2009;Zhao et al., 2007;Ge et al., 2012a;Sun et al., 2011b), all showed good correlation in time series with COA, e.g., $C_3H_3O^+$ (r = 0.75), $C_3H_5O^+$ (r = 0.61), $C_5H_8O^+$ (r = 0.89), $C_7H_{12}O^+$ (r = 0.70), and $C_6H_{10}O^+$ (r = 0.99) (Fig. S17 and Table 2) and COA was a major contributor to the signals of $C_5H_8O^+$, $C_6H_{10}O^+$, and $C_7H_{12}O^+$, accounting for 62%, 94%, and 67%, respectively, of their signals (Fig. S15). Finally, the ratios between *f*55 and *f*57 for OA in Seoul increased proportionally as the fractional contribution of COA to total OA increased (Fig. S18b), with a "V" shape indicated by the two edges defined by the COA and the HOA factors from several urban AMS data sets (Mohr et al., 2012). These observations all confirm the identification of COA at SMA.

3.3.2.3. Semi-volatile and low volatile oxygenated OA (SV-OOA and LV-OOA)

In addition to the two POA factors, two OOA factors were identified and were found to account for an average of 61% of the OA mass (Fig. S16a) with LV-OOA and SV-OOA being 34 and 27%, respectively. OOA is ubiquitous in the atmosphere and usually a dominant component of submicrometer particles (Jimenez et al., 2009;Zhang et al., 2007). SOA formation was more important in spring that in winter: OOA contributed an average 61% of the OA mass in this study but only 41% during winter. In addition, the average OOA concentration in this study was higher than in winter (5.9 vs. 4.9 μg m^{-3}).

CO_2^+ (*m/z* 44) and $C_2H_3O^+$ (*m/z* 43) were major fragments of oxidized organics and therefore frequently used as key tracers for identifying the presence of SOA in absence of biomass

burning influence. In this study, the time series of SV-OOA and LV-OOA correlated well with these ions, e.g., LV-OOA vs CO_2^+ (r = 0.78), SV-OOA vs $C_2H_3O^+$ (r = 0.89) (Figs. S17 and Table 2). As shown in the triangle plots in Fig. S18, SV-OOA (O/C = 0.56; H/C = 1.90) resides within the region representing fresher SOA, with a low f_{44}. The mass spectrum of SV-OOA is characterized by two prominent peaks, *m/z* 29 (mainly CHO^+) and *m/z* 43 (mainly $C_2H_3O^+$) (Fig. 8c). In addition, the SV-OOA show high fraction of $C_xH_yO_1^+$ family (41 %), most likely from carbonyl or alcohol functional groups, while much lower contribution of $C_xH_yO_2^+$ family (8.3 %), mainly from carboxylic functional groups (Fig. S16b). The diurnal variation of SV-OOA shows higher concentrations at night and lower concentrations at daytime with a small afternoon peak (Fig. 8g). The mass spectral features and diurnal variation of SV-OOA suggest that this factor was driven by the partitioning of semivolatile organics between gas and particle phase and that SV-OOA formation was facilitated by the high humidity and low temperature during nighttime. In addition, SV-OOA appeared to represent relatively fresh SOA formed from photochemical reactions during daytime (Docherty et al., 2011). Indeed, a decrease of the PBL height, thus less dilution, together with continued reactions of VOCs with the nighttime residual ozone (20–35 ppb on average; Fig. 3) and other oxidants (e.g., nitrate radical) might have played a role in the production of semivolatile secondary organic species at night. This kind of formation processes also suggests that SV-OOA was mostly formed locally. Indeed, the polar plot of SV-OOA showed that its high concentrations tended to be associated with lower wind speed.

On the other hand, the LV-OOA factor is characterized by high O/C ratio (=0.91) (Fig. 8d) and high f_{44} (14 %) (Fig. S18a), which are in similar range as those previously reported for aged and highly oxidized OA, including LV-OOAs, from various locations (e.g., Hayes et al., 2013;Mohr et al., 2012;Zhang et al., 2014;Ng et al., 2010). The diurnal profile of LV-OOA was different than SV-OOA as well, showing a gradual increase from 8:00 till late afternoon despite a rising PBL height (Fig. 8h). This diurnal pattern was very similar to O_x ($O_x = O_3+NO_2$) (Fig. 8). In fact, LV-OOA correlated positively with O_x (r = 0.57; Fig. S19) and the correlation was higher (r = 0.60; Fig. 9) between 10:00 and 16:00 when photochemical processing was intense. Note that a high organic period (May 20-May 23) was excluded in this correlation because it appeared to be driven by processes that were different than the other periods thus showed substantially higher LV-OOA/O_3 ratios than the rest of the study (Fig. 9). Details on this episode is discussed in section 3.4. Unless otherwise indicated, the high organic period (May 20-May 23) was excluded from the

Atmos. Chem. Phys. Discuss., https://doi.org/10.5194/acp-2017-947
Manuscript under review for journal Atmos. Chem. Phys.
Discussion started: 8 November 2017

O_x vs. OOA, LV-OOA and SV-OOA correlations. The relatively good correlation between LV-OOA and O_x during daytime indicates that LV-OOA corresponded to photochemically produced SOA (Fig. 8d). Furthermore, a gradual increase starting from ~08:00 till late afternoon indicated that the photochemical production was coupled with transport of air masses from regions outside of SMA. Indeed, the diurnal profile of ozone at the KIST site demonstrated a peak between 16:00–17:00 (Figs. 3,8) associated with southwesterly winds that transported ozone produced outside of SMA coupled with local daytime photochemical production. The high O/C (0.91) of the LV-OOA as well as a dispersed feature of its polar plot (Fig. S12) all support the regional secondary characteristics of LV-OOA.

Both SV-OOA and LV-OOA correlated positively with O_x during afternoon ($r = 0.53$, 0.6, respectively) and the correlation between total SOA (= LV-OOA + SV-OOA) and O_x was even higher ($r = 0.65$; Fig. 9a), indicating that afternoon SOA formation was strongly impacted by photochemistry. This observation is consistent with Herndon et al. (2008), who observed a strong correlation between OOA and O_x in photochemically processed urban plumes from Mexico City. The average OOA/O_x ratio observed in the present study (0.13 μg m^{-3}ppbv^{-1}) is within the ranges from those of Mexico City as well as other megacities including Tokyo, Los Angeles and Paris (0.13-0.18) (Zhang et al., 2015).

3.4 Impacts of Intense SOA formation on Haze

A sudden enhancement of PM_1 concentration from 11 to 44 μg m^{-3} occurred within 25 minutes between 17:09 to 17:15 on May 20 and PM_1 concentration continued to increase gradually to 71 μg m^{-3} till May 23. (Fig. 2h). As shown in Fig. S20, this enhancement was mainly driven by SOA formation, as both SV-OOA and LV-OOA increased sharply, as along with abrupt increases of biogenic and anthropogenic VOCs (e.g., isoprene and toluene). SOA remained elevated throughout the entire episode (May 20 17:00 to May 24 0:00) and on average accounted for 60 % of the PM_1 mass (Fig. 10a). Analysis of meteorological conditions (e.g., KORUS-AQ report, David Peterson, NRL) showed the stagnant conditions (e.g., slow wind speed and low mixing height) over South Korea during this period. The stagnant conditions in conjunction with high daytime O_3 mixing ratios (~ 78 ppb) and elevated VOCs concentrations might have accelerated the formation and accumulation of SOA during this episode. For example, as shown in Fig. 9, the correlation between SV-OOA and O_x during this period was tight and showed a substantially higher slope

Atmos. Chem. Phys. Discuss., https://doi.org/10.5194/acp-2017-947
Manuscript under review for journal Atmos. Chem. Phys.
Discussion started: 8 November 2017

(i.e., SV-OOA/O_x ratio = 0.11 μgm^{-3} ppb^{-1}) compared to the rest of the study (SV-OOA/O_x ratio = 0.053 μgm^{-3} ppb^{-1}) , indicating that SOA was formed more efficiently. However, the correlation of LV-OOA and total OOA = (LV-OOA+ SV-OOA) vs. O_x were both poor during this high OA episode, suggesting that in addition to photochemical reactions, other factors such as aging processes which occurred under the stagnant air flow condition likely have contributed to the high concentration of SOA as well.

On the other hand, the meteorological conditions during this event limited the formation of inorganic aerosol species. For example, according to backtrajectory analysis, air masses that arrived at the KIST site during this period (5/20 17:00 - 5/24 0:00) were predominantly from the east (Fig. 10c), where SO_2 emission sources are sparse, thus contained low sulfate concentration. In addition, the high temperature (24 ± 3 °C) and low RH (36 ± 11%) condition during this period was not favorable for nitrate aerosol formation. These results indicate that the SOA formation could be a leading cause for haze episode in SMA during springtime.

3.5 Regional and local influences on Haze events

Haze episodes occur often in East Asia including Seoul, Korea (e.g., (Kim et al., 2017) and references therein). Many investigations conducted in China suggest that the formation of severe haze pollution is a combined result of stagnant meteorological conditions associated with intense secondary aerosol formation, regional transport and primary emissions (Huang et al., 2014;Sun et al., 2014;Herndon et al., 2008;Sun et al., 2010;Wang et al., 2016a;Wang et al., 2016b;Zheng et al., 2015). Our investigation of the occurrence of haze episodes in Seoul during winter 2015 suggested that accumulation of primary pollutants and enhanced formation of secondary pollutants on a local scale were the main causes of wintertime haze episodes (Kim et al., 2017). However, the characteristics and the causes of haze episodes in the other seasons may be different than in winter. Therefore, more investigations are required to better design reduction strategies for PM in SMA. In this section, the lifecycle of a major springtime haze episode in SMA is discussed.

Shorter haze episodes with daily average PM_1 concentration higher than 30 $\mu g\ m^{-3}$ occurred several times during this study (Fig. 2). In addition, a severe haze episode lasted for 6 days from May 26 to May 31. Fig. 12 presents a case study of the full cycle of this haze episode, which is classified into four stages: Stage 1 (S1, May 24, 07:30–11:30) representing a clean period

Atmos. Chem. Phys. Discuss., https://doi.org/10.5194/acp-2017-947
Manuscript under review for journal Atmos. Chem. Phys.
Discussion started: 8 November 2017

(precipitation) before the haze, Stage 2 (S2, May 24 11:30– May 26 18:00) representing the formation stage of the haze, Stage 3 (S3, May 26 18:00- – May 31 24:00) representing the haze period with high concentrations of PM, and Stage 4 (S4, June 1 00:00–June 2 24:00) representing the clean of haze. This classification was mainly done based on changes in atmospheric conditions, i.e., precipitation, wind direction and speed.

On May 24, there was a short clean period (7:30 to 11:30; Period S1) when average PM_1 concentration was only 9 μg m^{-3} due to precipitation. After the precipitation, PM concentration started to increase substantially, accompanied with a change of aerosol composition. During both Period S1 and S2 (May 24, 11:30 – May 26, 18:00), the predominant wind direction was southwest (Fig. 11b). Analyses of the MODIS images (Fig. S21), backtrajectories, (Fig. S22) and meteorological conditions (Discover AQ report, Davis Peterson, NRL) all indicated direct transports of air masses from southwest, where large SO_2 emission sources are located. The change of PM_1 composition during Period S2 reflected the influence from such regional transport processes. For example, the mass fractions of species associated with regional sources, such as sulfate (28 vs 20% during entire period) and LV-OOA (18 vs 15%), increased (Fig. 11l, Table S2), whereas the fractions of local pollutants such as SV-OOA (5 vs 12%), HOA (5 vs 10%), COA (5 vs 7%) and BC (4 vs 7%) decreased compared to averaged PM_1 composition during entire period. In addition, the mass fraction of nitrate, one of the local secondary species, also enhanced (20 vs 17%), and this was mainly due to the gas-particle partitioning of HNO_3 and nighttime heterogeneous reactions in the nitrate formation facilitated by high RH (78%) and low temperature (18 °C) (Table S2). A good correlation (r^2=0.48) between nitrate and RH corroborates the role of aqueous processes (Fig. S23).

After S2, from May 26 – May 31 (Period S3), wind speed was reduced (Fig. 11, Table S2) and a more stagnant condition had developed over the SMA. High mass loadings of submicron aerosol species persisted due to lack of ventilation. In addition, similar to observation during a winter haze study at SMA (Kim et al., 2017), stagnant condition facilitated the accumulation of local sources and formation of local secondary species whereas prevented the transportation of regional species. For example, the mass fractions of all the local pollutants in PM_1 enhanced during S3, e.g., BC (6 % vs. 4% during S2), HOA (8% vs. 5%), COA (6% vs. 5%) and, nitrate (22% vs. 20%) whereas the fractions of regional pollutants decreased, e.g., sulfate (25% vs. 28%) and LV-OOA (9% vs. 18%), due to weaker regional impacts.

Atmos. Chem. Phys. Discuss., https://doi.org/10.5194/acp-2017-947
Manuscript under review for journal Atmos. Chem. Phys.
Discussion started: 8 November 2017

Atmospheric Chemistry and Physics Discussions

From June 1 to June 2 (Period S4), wind direction suddenly changed from west to north/northeast and average wind speed increased to 1.7 m/s (Table S2). This process cleaned out the atmosphere and reduced PM_1 concentration to an average value of 14 μg/m^3. OA was a major chemical species during this period, followed by sulfate and nitrate. During this time (S4), RH was low (~ 48%) which was less favorable for nighttime formation of nitrate. Furthermore, wind was predominantly from north, whereas main sources of SO_2 and sulfate were located in the west, resulting in a low concentration of sulfate in SMA.

Overall, unlike the haze episodes observed in winter, 2015(Kim et al., 2017), which were mainly due to local influences under stagnant conditions, the spring haze events observed in this study occurred due to a combination of regional and local effects. The evidences include 1) spring plumes were long range transported under the efficient conditions (high RH, low temp) for local species (nitrate) formation and 2) calm meteorology conditions followed by regional transportation promoted the formation and accumulation of species. Therefore, investigations and understanding on different cases of haze are required to better design reduction strategies.

4 Conclusions

Aerosol composition, size distribution, sources, and evolution processes were investigated using an HR-ToF-AMS and an SMPS in SMA, Korea, during spring 2016 as a part of the KORUS-AQ campaign. The average PM_1 concentration was 22.1 μg m^{-3} and the total mass was dominated by organics (44%) and secondary inorganic species such as sulfate (20%) and nitrate (17%). Secondary materials (i.e., nitrate, sulfate, ammonium, SV-OOA and LV-OOA) together accounted for 76% of the PM_1 mass, with the remainder being primary materials (HOA, COA, and BC), indicating that air quality in SMA during spring time is influenced strongly by secondary aerosol formation.

Meteorological conditions and various emission sources influenced the concentrations, compositions, size distributions, and chemical composition of aerosol particles in SMA. Sulfate was found to be mainly associated with regional transport and to a lesser degree formed by local photochemical processes during late afternoon. In contrast, nitrate was formed more locally due to intense urban emissions of NO_x coupled with elevated ozone concentrations and enhanced gas to particle partition during nighttime. Aqueous-phase processing under high humidity and low temperature might have increased particulate nitrate concentrations occasionally as well. The two

types of SOA showed significantly different features of diurnal patterns which indicated that both were formed by photochemical reactions, but SV-OOA represented freshly formed local SOA and was also enhanced by gas-to-particle partition during nighttime. On the other hand, LV-OOA enhanced in late afternoon, similar to the behavior of ozone, indicating that LV-OOA is photochemically generated and regionally transported.

Based on detailed analyses of the haze periods in this study, we found that meteorological conditions played a significant role in controlling air quality in SMA. However, unlike in winter 2015, when haze episodes were found to occur mainly under stagnant conditions due to local influences, the springtime haze events occurred due to a combination of regional transport and local emissions. For example, a haze episode was found to begin with long-range transport of plumes followed by stagnant conditions as well as meteorological conditions favorable for secondary inorganic aerosol formation. The sequential occurrence of plume transport and stagnant periods led to more severe air pollution that lasted for a longer period. Another episode dominated by OA started with the transport of plumes enriched of both PM_1 and VOCs from the west and followed by stagnant conditions with low mixing height. During this episode, inorganic aerosol formation was limited since SO_2 concentration was low and the meteorological condition was not favorable for nitrate aerosol formation (e.g., high temperature and low RH). However, due to high concentrations of VOCs and O_3, intense formation of SOA was observed. These results indicate that the high PM pollution in SMA during springtime was caused by a combination of factors, including local emissions, regional transport, and meteorological conditions which promote secondary aerosol formation or accumulation of pollutants. Therefore, understanding the haze episode followed by efficient strategies to remove precursors are important to control the air pollution.

Acknowledgments

This work was supported by the Korea Institute of Science and Technology (KIST) and Basic Science Research Program through the National Research Foundation of Korea (NRF) funded by the Ministry of Science and ICT (2017R1A2B3004950). QZ acknowledges the Changjiang Scholars program of the Chinese Ministry of Education.

Atmos. Chem. Phys. Discuss., https://doi.org/10.5194/acp-2017-947
Manuscript under review for journal Atmos. Chem. Phys.
Discussion started: 8 November 2017

Atmospheric Chemistry and Physics Discussions

References

Adhikary, B., Carmichael, G. R., Kulkarni, S., Wei, C., Tang, Y., D'Allura, A., Mena-Carrasco, M., Streets, D. G., Zhang, Q., Pierce, R. B., Al-Saadi, J. A., Emmons, L. K., Pfister, G. G., Avery, M. A., Barrick, J. D., Blake, D. R., Brune, W. H., Cohen, R. C., Dibb, J. E., Fried, A., Heikes, B. G., Huey, L. G., O'Sullivan, D. W., Sachse, G. W., Shetter, R. E., Singh, H. B., Campos, T. L., Cantrell, C. A., Flocke, F. M., Dunlea, E. J., Jimenez, J. L., Weinheimer, A. J., Crounse, J. D., Wennberg, P. O., Schauer, J. J., Stone, E. A., Jaffe, D. A., and Reidmiller, D. R.: A regional scale modeling analysis of aerosol and trace gas distributions over the eastern Pacific during the INTEX-B field campaign, Atmospheric Chemistry and Physics, 10, 2091-2115, 2010.

Aiken, A. C., Decarlo, P. F., Kroll, J. H., Worsnop, D. R., Huffman, J. A., Docherty, K. S., Ulbrich, I. M., Mohr, C., Kimmel, J. R., Sueper, D., Sun, Y., Zhang, Q., Trimborn, A., Northway, M., Ziemann, P. J., Canagaratna, M. R., Onasch, T. B., Alfarra, M. R., Prevot, A. S. H., Dommen, J., Duplissy, J., Metzger, A., Baltensperger, U., and Jimenez, J. L.: O/C and OM/OC ratios of primary, secondary, and ambient organic aerosols with high-resolution time-of-flight aerosol mass spectrometry, Environmental Science & Technology, 42, 4478-4485, 10.1021/es703009q, 2008.

Aiken, A. C., Salcedo, D., Cubison, M. J., Huffman, J. A., DeCarlo, P. F., Ulbrich, I. M., Docherty, K. S., Sueper, D., Kimmel, J. R., Worsnop, D. R., Trimborn, A., Northway, M., Stone, E. A., Schauer, J. J., Volkamer, R. M., Fortner, E., de Foy, B., Wang, J., Laskin, A., Shutthanandan, V., Zheng, J., Zhang, R., Gaffney, J., Marley, N. A., Paredes-Miranda, G., Arnott, W. P., Molina, L. T., Sosa, G., and Jimenez, J. L.: Mexico City aerosol analysis during MILAGRO using high resolution aerosol mass spectrometry at the urban supersite (T0) – Part 1: Fine particle composition and organic source apportionment, Atmospheric Chemistry and Physics, 9, 6633-6653, 10.5194/acp-9-6633-2009, 2009.

Alfarra, M. R., Prevot, A. S. H., Szidat, S., Sandradewi, J., Weimer, S., Lanz, V. A., Schreiber, D., Mohr, M., and Baltensperger, U.: Identification of the Mass Spectral Signature of Organic Aerosols from Wood Burning Emissions, Environmental Science & Technology, 41, 5770-5777, 10.1021/es062289b, 2007.

Allan, J. D., Delia, A. E., Coe, H., Bower, K. N., Alfarra, M. R., Jimenez, J. L., Middlebrook, A. M., Drewnick, F., Onasch, T. B., Canagaratna, M. R., Jayne, J. T., and Worsnop, D. R.: A generalised method for the extraction of chemically resolved mass spectra from aerodyne aerosol mass spectrometer data, J Aerosol Sci, 35, 909-922, 10.1016/j.jaerosci.2004.02.007, 2004.

Ban-Weiss, G. A., McLaughlin, J. P., Harley, R. A., Lunden, M. M., Kirchstetter, T. W., Kean, A. J., Strawa, A. W., Stevenson, E. D., and Kendall, G. R.: Long-term changes in emissions of nitrogen oxides and particulate matter from on-road gasoline and diesel vehicles, Atmospheric Environment, 42, 220-232, 10.1016/j.atmosenv.2007.09.049, 2008.

Canagaratna, M. R., Jayne, J. T., Jimenez, J. L., Allan, J. D., Alfarra, M. R., Zhang, Q., Onasch, T. B., Drewnick, F., Coe, H., Middlebrook, A., Delia, A., Williams, L. R., Trimborn, A. M., Northway, M. J., DeCarlo, P. F., Kolb, C. E., Davidovits, P., and Worsnop, D. R.: Chemical and microphysical characterization of ambient aerosols with the aerodyne aerosol mass spectrometer, Mass Spectrometry Reviews, 26, 185-222, 10.1002/mas.20115, 2007.

Canagaratna, M. R., Jimenez, J. L., Kroll, J. H., Chen, Q., Kessler, S. H., Massoli, P., Hildebrandt Ruiz, L., Fortner, E., Williams, L. R., Wilson, K. R., Surratt, J. D., Donahue, N. M., Jayne, J. T., and Worsnop, D. R.: Elemental ratio measurements of organic compounds using aerosol mass spectrometry: characterization, improved calibration, and implications, Atmospheric Chemistry and Physics, 15, 253-272, 10.5194/acp-15-253-2015, 2015.

Cao, J.-j., Wang, Q.-y., Chow, J. C., Watson, J. G., Tie, X.-x., Shen, Z.-x., Wang, P., and An, Z.-s.: Impacts of aerosol compositions on visibility impairment in Xi'an, China, Atmospheric Environment, 59, 559-566, 10.1016/j.atmosenv.2012.05.036, 2012.

Collier, S., S. Zhou, T. Kuwayama, S. Forestieri, J. Brady, M. Zhang, M. Kleeman, C. Cappa, T. Bertram, and Q. Zhang: Organic PM Emissions from Vehicles: composition, O/C ratio, and dependence on PM concentration, Aerosol Science and Technology, 49, 11, 2015.

DeCarlo, P. F., Slowik, J. G., Worsnop, D. R., Davidovits, P., and Jimenez, J. L.: Particle morphology and density characterization by combined mobility and aerodynamic diameter measurements. Part 1: Theory, Aerosol Science and Technology, 38, 1185-1205, Doi 10.1080/02786820590928897, 2004.

DeCarlo, P. F., Kimmel, J. R., Trimborn, A., Northway, M. J., Jayne, J. T., Aiken, A. C., Gonin, M., Fuhrer, K., Horvath, T., Docherty, K. S., Worsnop, D. R., and Jimenez, J. L.: Field-deployable, high-resolution, time-of-flight aerosol mass spectrometer, Analytical Chemistry, 78, 8281-8289, 10.1021/ac061249n, 2006.

Docherty, K. S., Aiken, A. C., Huffman, J. A., Ulbrich, I. M., DeCarlo, P. F., Sueper, D., Worsnop, D. R., Snyder, D. C., Grover, B. D., Eatough, D. J., Goldstein, A. H., Ziemann, P. J., and Jimenez, J. L.: The 2005 Study of Organic Aerosols at Riverside (SOAR-1): instrumental intercomparisons and fine particle composition, Atmospheric Chemistry and Physics Discussions, 11, 6301-6362, 10.5194/acpd-11-6301-2011, 2011.

Draxler, R. R., Stunder, B., Rolph, G., Stein, A., and Taylor, A.: HYSPLIT_4 User's Guide, available at http://www.arl.noaa.gov/documents/reports/hysplit_user_guide.pdf, NOAA Air Resources Laboratory, Silver Spring,Maryland, USA

2012.

Draxler, R. R. a. H., G. D.: Description of the HYSPLIT_4 modeling system, available at: http://www.arl.noaa.gov/documents/reports/arl-224.pdf (last access: 5 January 2014),NOAA Air Resources Laboratory, Silver Spring, Maryland,USA, 1997.

Ge, X., Setyan, A., Sun, Y., and Zhang, Q.: Primary and secondary organic aerosols in Fresno, California during wintertime: Results from high resolution aerosol mass spectrometry, Journal of Geophysical Research-Atmospheres, 117, 10.1029/2012jd018026, 2012a.

Ge, X. L., Zhang, Q., Sun, Y. L., Ruehl, C. R., and Setyan, A.: Effect of aqueous-phase processing on aerosol chemistry and size distributions in Fresno, California, during wintertime, Environ. Chem., 9, 221-235, 10.1071/en11168, 2012b.

Guo, S., Hu, M., Zamora, M. L., Peng, J., Shang, D., Zheng, J., Du, Z., Wu, Z., Shao, M., Zeng, L., Molina, M. J., and Zhang, R.: Elucidating severe urban haze formation in China, Proceedings of the National Academy of Sciences, 111, 17373-17378, 10.1073/pnas.1419604111, 2014.

Harrison, R. M., and Yin, J.: Particulate matter in the atmosphere: which particle properties are important for its effects on health?, Science of the Total Environment, 249, 85-101, http://dx.doi.org/10.1016/S0048-9697(99)00513-6, 2000.

Hayes, P. L., Ortega, A. M., Cubison, M. J., Froyd, K. D., Zhao, Y., Cliff, S. S., Hu, W. W., Toohey, D. W., Flynn, J. H., Lefer, B. L., Grossberg, N., Alvarez, S., Rappenglueck, B., Taylor, J. W., Allan, J. D., Holloway, J. S., Gilman, J. B., Kuster, W. C., De Gouw, J. A., Massoli, P., Zhang, X., Liu, J., Weber, R. J., Corrigan, A. L., Russell, L. M., Isaacman, G., Worton, D. R., Kreisberg, N. M., Goldstein, A. H., Thalman, R., Waxman, E. M., Volkamer, R., Lin, Y. H., Surratt, J. D., Kleindienst, T. E., Offenberg, J. H., Dusanter, S., Griffith, S., Stevens, P. S., Brioude, J., Angevine, W. M., and Jimenez, J. L.: Organic aerosol composition and sources in Pasadena, California, during the 2010 CalNex campaign, Journal of Geophysical Research-Atmospheres, 118, 9233-9257, 10.1002/jgrd.50530, 2013.

He, J., Zielinska, B., and Balasubramanian, R.: Composition of semi-volatile organic compounds in the urban atmosphere of Singapore: influence of biomass burning, Atmospheric Chemistry and Physics, 10, 11401-11413, 10.5194/acp-10-11401-2010, 2010.

He, L. Y., Hu, M., Huang, X. F., Yu, B. D., Zhang, Y. H., and Liu, D. Q.: Measurement of emissions of fine particulate organic matter from Chinese cooking, Atmospheric Environment, 38, 6557-6564, 10.1016/j.atmosenv.2004.08.034, 2004.

Heo, J. B., Hopke, P. K., and Yi, S. M.: Source apportionment of PM2.5 in Seoul, Korea, Atmospheric Chemistry and Physics, 9, 4957-4971, 2009.

Herndon, S. C., Onasch, T. B., Wood, E. C., Kroll, J. H., Canagaratna, M. R., Jayne, J. T., Zavala, M. A., Knighton, W. B., Mazzoleni, C., Dubey, M. K., Ulbrich, I. M., Jimenez, J. L., Seila, R., Gouw, J. A. d., Foy, B. d., Fast, J., Molina, L. T., Kolb, C. E., and Worsnop, D. R.: The correlation of secondary organic aerosol with odd oxygen in Mexico City, , Geophys. Res. Lett., 35, 2008.

Hu, W., Hu, M., Hu, W., Jimenez, J. L., Yuan, B., Chen, W., Wang, M., Wu, Y., Chen, C., Wang, Z., Peng, J., Zeng, L., and Shao, M.: Chemical composition, sources, and aging process of submicron aerosols in Beijing: Contrast between summer and winter, Journal of Geophysical Research: Atmospheres, 121, 1955-1977, 10.1002/2015JD024020, 2016.

Huang, R.-J., Zhang, Y., Bozzetti, C., Ho, K.-F., Cao, J.-J., Han, Y., Daellenbach, K. R., Slowik, J. G., Platt, S. M., Canonaco, F., Zotter, P., Wolf, R., Pieber, S. M., Bruns, E. A., Crippa, M., Ciarelli, G., Piazzalunga, A., Schwikowski, M., Abbaszade, G., Schnelle-Kreis, J., Zimmermann, R., An, Z., Szidat, S., Baltensperger, U., El Haddad, I., and Prevot, A. S. H.: High secondary aerosol contribution to particulate pollution during haze events in China, Nature, 514, 218-222, 10.1038/nature13774, 2014.

Huang, X. F., He, L. Y., Hu, M., Canagaratna, M. R., Sun, Y., Zhang, Q., Zhu, T., Xue, L., Zeng, L. W., Liu, X. G., Zhang, Y. H., Jayne, J. T., Ng, N. L., and Worsnop, D. R.: Highly time-resolved chemical characterization of atmospheric submicron particles during 2008 Beijing Olympic Games using an Aerodyne High-Resolution Aerosol Mass Spectrometer, Atmospheric Chemistry and Physics, 10, 8933-8945, 10.5194/acp-10-8933-2010, 2010.

IPCC: Summary for policymakers, in: Climate Change 2013: The Physical Science Basis. Contribution of Working Group 1 to the Fifth Assessment Report of the Intergovernmental Panel on Climate Change, edited by: Stocker, T. F., Qin, D., Plattner, G.-K., Tignor, M., Allen, S. K., Boschung, J., Nauels, A., Xia, Y., Bex, V., and Midgley, P. M., Cambridge University Press, Cambridge, UK, New York, NY, USA, 3-29, 2013.

Jimenez, J. L., Jayne, J. T., Shi, Q., Kolb, C. E., Worsnop, D. R., Yourshaw, I., Seinfeld, J. H., Flagan, R. C., Zhang, X. F., Smith, K. A., Morris, J. W., and Davidovits, P.: Ambient aerosol sampling using the Aerodyne Aerosol Mass Spectrometer, Journal of Geophysical Research-Atmospheres, 108, -, 10.1029/2001jd001213, 2003.

Jimenez, J. L., Canagaratna, M. R., Donahue, N. M., Prevot, A. S. H., Zhang, Q., Kroll, J. H., DeCarlo, P. F., Allan, J. D., Coe, H., Ng, N. L., Aiken, A. C., Docherty, K. S., Ulbrich, I. M., Grieshop, A. P., Robinson, A. L., Duplissy, J., Smith, J. D., Wilson, K. R., Lanz, V. A., Hueglin, C., Sun, Y. L., Tian, J., Laaksonen, A., Raatikainen, T., Rautiainen, J., Vaattovaara, P., Ehn, M., Kulmala, M., Tomlinson, J. M., Collins, D. R., Cubison, M. J., Dunlea, E. J., Huffman, J. A., Onasch, T. B., Alfarra, M. R., Williams, P. I., Bower, K., Kondo, Y., Schneider, J., Drewnick, F., Borrmann, S., Weimer, S., Demerjian, K., Salcedo, D., Cottrell, L., Griffin, R., Takami, A., Miyoshi, T., Hatakeyama, S., Shimono, A., Sun, J. Y., Zhang, Y. M., Dzepina, K., Kimmel, J. R., Sueper, D., Jayne, J. T., Herndon, S. C., Trimborn, A. M., Williams, L. R., Wood, E. C., Middlebrook, A. M., Kolb, C. E., Baltensperger, U., and Worsnop, D. R.: Evolution of Organic Aerosols in the Atmosphere, Science, 326, 1525-1529, 10.1126/science.1180353, 2009.

Kaneyasu, N., Ohta, S., and Murao, N.: Seasonal variation in the chemical composition of atmospheric aerosols and gaseous species in SAPPORO, JAPAN, Atmospheric Environment, 29, 1559-1568, 10.1016/1352-2310(94)00356-p, 1995.

Kim, E., Hopke, P. K., and Edgerton, E. S.: Source identification of Atlanta aerosol by positive matrix factorization, Journal of the Air & Waste Management Association, 53, 731-739, 2003.

Kim, H., Zhang, Q., Bae, G. N., Kim, J. Y., and Lee, S. B.: Sources and atmospheric processing of winter aerosols in Seoul, Korea: insights from real-time measurements using a high-resolution aerosol mass spectrometer, Atmos. Chem. Phys., 17, 2009-2033, 10.5194/acp-17-2009-2017, 2017.

Kim, S.-W., Choi, I.-J., and Yoon, S.-C.: A multi-year analysis of clear-sky aerosol optical properties and direct radiative forcing at Gosan, Korea (2001–2008), Atmospheric Research, 95, 8, 2010.

Kim, Y., Kim, S.-W., Yoon, S.-C., Kim, M.-H., and Park, K.-H.: Aerosol properties and associated regional meteorology during winter pollution event at Gosan climate observatory, Korea, Atmospheric Environment, 85, 9-17, 10.1016/j.atmosenv.2013.11.041, 2014.

Kuwata, M., Zorn, S. R., and Martin, S. T.: Using Elemental Ratios to Predict the Density of Organic Material Composed of Carbon, Hydrogen, and Oxygen, Environmental Science & Technology, 46, 787-794, 10.1021/es202525q, 2012.

Lanz, V. A., Alfarra, M. R., Baltensperger, U., Buchmann, B., Hueglin, C., and Prevot, A. S. H.: Source apportionment of submicron organic aerosols at an urban site by factor analytical modelling of aerosol mass spectra, Atmospheric Chemistry and Physics, 7, 1503-1522, 2007.

Lanz, V. A., Alfarra, M. R., Baltensperger, U., Buchmann, B., Hueglin, C., Szidat, S., Wehrli, M. N., Wacker, L., Weimer, S., Caseiro, A., Puxbaum, H., and Prevot, A. S. H.: Source Attribution of Submicron Organic Aerosols during Wintertime Inversions by Advanced Factor Analysis of Aerosol Mass Spectra, Environmental Science & Technology, 42, 214-220, 10.1021/es0707207, 2008.

Middlebrook, A. M., Bahreini, R., Jimenez, J. L., and Canagaratna, M. R.: Evaluation of Composition-Dependent Collection Efficiencies for the Aerodyne Aerosol Mass Spectrometer using Field Data, Aerosol Science and Technology, 46, 258-271, 10.1080/02786826.2011.620041, 2012.

Mohr, C., Huffman, J. A., Cubison, M. J., Aiken, A. C., Docherty, K. S., Kimmel, J. R., Ulbrich, I. M., Hannigan, M., and Jimenez, J. L.: Characterization of Primary Organic Aerosol Emissions from Meat Cooking, Trash Burning, and Motor Vehicles with High-Resolution Aerosol Mass Spectrometry and Comparison with Ambient and Chamber Observations, Environmental Science & Technology, 43, 2443-2449, Doi 10.1021/Es8011518, 2009.

Mohr, C., DeCarlo, P. F., Heringa, M. F., Chirico, R., Slowik, J. G., Richter, R., Reche, C., Alastuey, A., Querol, X., Seco, R., Penuelas, J., Jimenez, J. L., Crippa, M., Zimmermann, R., Baltensperger, U., and Prevot, A. S. H.: Identification and quantification of organic aerosol from cooking and other sources in Barcelona using aerosol mass spectrometer data, Atmospheric Chemistry and Physics, 12, 1649-1665, 10.5194/acp-12-1649-2012, 2012.

Molina, M. J., and Molina, L.T.: Megacities and Atmospheric Pollution, Air and Waste Manage. Assoc., 36, 2004.

Morgan, W. T., Allan, J. D., Bower, K. N., Highwood, E. J., Liu, D., McMeeking, G. R., Northway, M. J., Williams, P. I., Krejci, R., and Coe, H.: Airborne measurements of the spatial distribution of aerosol chemical composition across Europe and evolution of the organic fraction, Atmospheric Chemistry and Physics, 10, 4065-4083, 10.5194/acp-10-4065-2010, 2010.

Ng, N. L., Canagaratna, M. R., Zhang, Q., Jimenez, J. L., Tian, J., Ulbrich, I. M., Kroll, J. H., Docherty, K. S., Chhabra, P. S., Bahreini, R., Murphy, S. M., Seinfeld, J. H., Hildebrandt, L., Donahue, N. M., DeCarlo, P. F., Lanz, V. A., Prevot, A. S. H., Dinar, E., Rudich, Y., and Worsnop, D. R.: Organic aerosol components observed in Northern Hemispheric datasets from Aerosol Mass Spectrometry, Atmospheric Chemistry and Physics, 10, 4625-4641, 10.5194/acp-10-4625-2010, 2010.

Ng, N. L., Canagaratna, M. R., Jimenez, J. L., Zhang, Q., Ulbrich, I. M., and Worsnop, D. R.: Real-Time Methods for Estimating Organic Component Mass Concentrations from Aerosol Mass Spectrometer Data, Environmental Science & Technology, 45, 910-916, Doi 10.1021/Es102951k, 2011.

Paatero, P., and Tapper, U.: Positive matrix factorization - A Nonnegative factor model with optimal utilization of error-estimates of data values, Environmetrics, 5, 111-126, 10.1002/env.3170050203, 1994.

Pope III, C. A., and Dockery, D. W.: Health Effects of Fine Particulate Air Pollution: Lines that Connect, Journal of the Air & Waste Management Association, 56, 709-742, 2006.

Pöschl, U.: Atmospheric Aerosols: Composition, Transformation, Climate and Health Effects, Angewandte Chemie International Edition, 44, 7520-7540, 10.1002/anie.200501122, 2005.

Prabhakar, G., Parworth, C., Zhang, X., Kim, H., Young, D., Beyersdorf, A. J., Ziemba, L. D., Nowak, J. B., Bertram, T. H., Faloona, I. C., Zhang, Q., and Cappa, C. D.: Observational assessment of the role of nocturnal residual-layer chemistry in determining daytime surface particulate nitrate concentrations, Atmos. Chem. Phys. Discuss., 2017, 1-58, 10.5194/acp-2017-512, 2017.

Seinfeld, J. H., and Pandis, S. N.: Atmospheric Chemistry and Physics: From Air Pollution to Climate Change, 2nd ed., John Wiley & Sons, New York, 1232 pp., 2006.

Setyan, A., Zhang, Q., Merkel, M., Knighton, W. B., Sun, Y., Song, C., Shilling, J. E., Onasch, T. B., Herndon, S. C., Worsnop, D. R., Fast, J. D., Zaveri, R. A., Berg, L. K., Wiedensohler, A., Flowers, B. A., Dubey, M. K., and Subramanian, R.: Characterization of submicron particles influenced by mixed biogenic and anthropogenic emissions using high-resolution aerosol mass spectrometry: results from CARES, Atmospheric Chemistry and Physics, 12, 8131-8156, 10.5194/acp-12-8131-2012, 2012.

Sun, J., Zhang, Q., Canagaratna, M. R., Zhang, Y., Ng, N. L., Sun, Y., Jayne, J. T., Zhang, X., Zhang, X., and Worsnop, D. R.: Highly time- and size-resolved characterization of submicron aerosol particles in Beijing using an Aerodyne Aerosol Mass Spectrometer, Atmospheric Environment, 44, 131-140, 10.1016/j.atmosenv.2009.03.020, 2010.

Sun, Y., Jiang, Q., Wang, Z., Fu, P., Li, J., Yang, T., and Yin, Y.: Investigation of the sources and evolution processes of severe haze pollution in Beijing in January 2013, Journal of Geophysical Research-Atmospheres, 119, 4380-4398, 10.1002/2014jd021641, 2014.

Sun, Y., Jiang, Q., Xu, Y., Ma, Y., Zhang, Y., Liu, X., Li, W., Wang, F., Li, J., Wang, P., and Li, Z.: Aerosol characterization over the North China Plain: Haze life cycle and biomass burning impacts in summer, Journal of Geophysical Research: Atmospheres, 121, 2508-2521, 10.1002/2015jd024261, 2016.

Sun, Y. L., Zhang, Q., Schwab, J. J., Chen, W. N., Bae, M. S., Lin, Y. C., Hung, H. M., and Demerjian, K. L.: A case study of aerosol processing and evolution in summer in New York City, Atmos. Chem. Phys., 11, 12737-12750, 10.5194/acp-11-12737-2011, 2011a.

Sun, Y. L., Zhang, Q., Schwab, J. J., Demerjian, K. L., Chen, W. N., Bae, M. S., Hung, H. M., Hogrefe, O., Frank, B., Rattigan, O. V., and Lin, Y. C.: Characterization of the sources and processes of organic and inorganic aerosols in New York city with a high-resolution time-of-flight aerosol mass apectrometer, Atmospheric Chemistry and Physics, 11, 1581-1602, 10.5194/acp-11-1581-2011, 2011b.

Sun, Y. L., Zhang, Q., Schwab, J. J., Yang, T., Ng, N. L., and Demerjian, K. L.: Factor analysis of combined organic and inorganic aerosol mass spectra from high resolution aerosol mass spectrometer measurements, Atmospheric Chemistry and Physics, 12, 8537-8551, 10.5194/acp-12-8537-2012, 2012.

Ulbrich, I. M., Canagaratna, M. R., Zhang, Q., Worsnop, D. R., and Jimenez, J. L.: Interpretation of organic components from Positive Matrix Factorization of aerosol mass spectrometric data, Atmospheric Chemistry and Physics, 9, 2891-2918, 10.5194/acp-9-2891-2009, 2009.

Wang, D., Zhou, B., Fu, Q., Zhao, Q., Zhang, Q., Chen, J., Yang, X., Duan, Y., and Li, J.: Intense secondary aerosol formation due to strong atmospheric photochemical reactions in summer: observations at a rural site in eastern Yangtze River Delta of China, The Science of the total environment, 571, 1454-1466, 10.1016/j.scitotenv.2016.06.212, 2016a.

Wang, J., Ge, X., Chen, Y., Shen, Y., Zhang, Q., Sun, Y., Xu, J., Ge, S., Yu, H., and Chen, M.: Highly time-resolved urban aerosol characteristics during springtime in Yangtze River Delta, China: insights from soot particle aerosol mass spectrometry, Atmos. Chem. Phys., 16, 9109-9127, 10.5194/acp-16-9109-2016, 2016b.

Xu, J., Zhang, Q., Chen, M., Ge, X., Ren, J., and Qin, D.: Chemical composition, sources, and processes of urban aerosols during summertime in northwest China: insights from high-resolution aerosol mass spectrometry, Atmospheric Chemistry and Physics, 14, 12593-12611, 10.5194/acp-14-12593-2014, 2014.

Young, D. E., Allan, J. D., Williams, P. I., Green, D. C., Flynn, M. J., Harrison, R. M., Yin, J., Gallagher, M. W., and Coe, H.: Investigating the annual behaviour of submicron secondary inorganic and organic aerosols in London, Atmospheric Chemistry and Physics, 15, 6351-6366, 10.5194/acp-15-6351-2015, 2015.

Young, D. E., Kim, H., Parworth, C., Zhou, S., Zhang, X., Cappa, C. D., Seco, R., Kim, S., and Zhang, Q.: Influences of emission sources and meteorology on aerosol chemistry in a polluted urban environment: results from DISCOVER-AQ California, Atmos. Chem. Phys., 16, 5427-5451, 10.5194/acp-16-5427-2016, 2016.

Zhang, J. K., Sun, Y., Liu, Z. R., Ji, D. S., Hu, B., Liu, Q., and Wang, Y. S.: Characterization of submicron aerosols during a month of serious pollution in Beijing, 2013, Atmospheric Chemistry and Physics, 14, 2887-2903, 10.5194/acp-14-2887-2014, 2014.

Zhang, Q., Alfarra, M. R., Worsnop, D. R., Allan, J. D., Coe, H., Canagaratna, M. R., and Jimenez, J. L.: Deconvolution and quantification of hydrocarbon-like and oxygenated organic aerosols based on aerosol mass spectrometry, Environmental Science & Technology, 39, 4938-4952, 10.1021/Es048568l, 2005a.

Zhang, Q., Canagaratna, M. R., Jayne, J. T., Worsnop, D. R., and Jimenez, J. L.: Time- and size-resolved chemical composition of submicron particles in Pittsburgh: Implications for aerosol sources and processes, Journal of Geophysical Research-Atmospheres, 110, 10.1029/2004jd004649, 2005b.

Zhang, Q., Worsnop, D. R., Canagaratna, M. R., and Jimenez, J. L.: Hydrocarbon-like and oxygenated organic aerosols in Pittsburgh: insights into sources and processes of organic aerosols, Atmospheric Chemistry and Physics, 5, 3289-3311, 2005c.

Zhang, Q., Jimenez, J. L., Canagaratna, M. R., Allan, J. D., Coe, H., Ulbrich, I., Alfarra, M. R., Takami, A., Middlebrook, A. M., Sun, Y. L., Dzepina, K., Dunlea, E., Docherty, K., DeCarlo, P. F., Salcedo, D., Onasch, T., Jayne, J. T., Miyoshi, T., Shimono, A., Hatakeyama, S., Takegawa, N., Kondo, Y., Schneider, J., Drewnick, F., Borrmann, S., Weimer, S., Demerjian, K., Williams, P., Bower, K., Bahreini, R., Cottrell, L., Griffin, R. J., Rautiainen, J., Sun, J. Y., Zhang, Y. M., and Worsnop, D. R.: Ubiquity and dominance of oxygenated species in organic aerosols in anthropogenically-influenced Northern Hemisphere midlatitudes, Geophysical Research Letters, 34, L13801, Artn L13801, Doi 10.1029/2007gl029979, 2007.

Zhang, Q., Jimenez, J. L., Canagaratna, M. R., Ulbrich, I. M., Ng, N. L., Worsnop, D. R., and Sun, Y.: Understanding atmospheric organic aerosols via factor analysis of aerosol mass spectrometry: a review, Analytical and bioanalytical chemistry, 401, 3045-3067, 10.1007/s00216-011-5355-y, 2011.

Zhang, Q. J., Beekmann, M., Freney, E., Sellegri, K., Pichon, J. M., Schwarzenboeck, A., Colomb, A., Bourrianne, T., Michoud, V., and Borbon, A.: Formation of secondary organic aerosol in the Paris

pollution plume and its impact on surrounding regions, Atmospheric Chemistry and Physics, 15, 13973-13992, 10.5194/acp-15-13973-2015, 2015.

Zhao, Y., Hu, M., Slanina, S., and Zhang, Y.: Chemical compositions of fine particulate organic matter emitted from Chinese cooking, Environmental Science & Technology, 41, 99-105, 10.1021/es0614518, 2007.

Zheng, G. J., Duan, F. K., Su, H., Ma, Y. L., Cheng, Y., Zheng, B., Zhang, Q., Huang, T., Kimoto, T., Chang, D., Pöschl, U., Cheng, Y. F., and He, K. B.: Exploring the severe winter haze in Beijing: the impact of synoptic weather, regional transport and heterogeneous reactions, Atmos. Chem. Phys., 15, 2969-2983, 10.5194/acp-15-2969-2015, 2015.

Zhou, S., Collier, S., Xu, J. Z., Mei, F., Wang, J., Lee, Y. N., Sedlacek, A. J., Springston, S. R., Sun, Y. L., and Zhang, Q.: Influences of upwind emission sources and atmospheric processing on aerosol chemistry and properties at a rural location in the Northeastern US, Journal of Geophysical Research-Atmospheres, 121, 6049-6065, 10.1002/2015jd024568, 2016.

Zhou, S., Collier, S., Jaffe, D. A., Briggs, N. L., Hee, J., Sedlacek Iii, A. J., Kleinman, L., Onasch, T. B., and Zhang, Q.: Regional influence of wildfires on aerosol chemistry in the western US and insights into atmospheric aging of biomass burning organic aerosol, Atmos. Chem. Phys., 17, 2477-2493, 10.5194/acp-17-2477-2017, 2017.

Atmos. Chem. Phys. Discuss., https://doi.org/10.5194/acp-2017-947
Manuscript under review for journal Atmos. Chem. Phys.
Discussion started: 8 November 2017

Atmospheric Chemistry and Physics Discussions

Tables

Table 1. Average (± 1 standard deviation), minimum and maximum concentrations of the particulate matter (PM_1) species and the total PM_1 mass over the whole campaign, and the average contribution of each of the PM_1 species to the total PM_1 mass.

	Average conc. ± one standard deviation (μg m^{-3})	Minimum conc. (μg m^{-3})	Maximum conc. (μg m^{-3})	Fraction of total PM_1 (%)	Detection limit (3min) (μg m^{-3})
Organics	9.76 ± 5.27	0.26	38.8	44	0.04
Nitrate	3.78 ± 4.20	0.05	23.4	17	0.01
Sulfate	4.40 ± 3.26	0.19	20.6	20	0.01
Ammonium	2.56 ± 2.16	0.05	11.7	12	0.03
Chloride	0.04 ± 0.05	0	0.62	0	0.01
Black carbon	1.52 ± 0.82	0	7.81	7	0.1
Total PM_1	22.1 ± 13.0	0.76	71.3	-	0.05

Atmos. Chem. Phys. Discuss., https://doi.org/10.5194/acp-2017-947
Manuscript under review for journal Atmos. Chem. Phys.
Discussion started: 8 November 2017

Atmospheric Chemistry and Physics Discussions

Table 2. Correlation coefficient (Pearson's r) for the linear regressions between organic aerosol (OA) factors (including the sum of primary factors (primary OA (POA) = hydrocarbon like OA (HOA) + cooking OA (COA) + biomass burning OA (BBOA)), as well as the sum of the oxidized factors (oxidized OA (OOA) = semi-volatile OOA (SV-OOA) + low volatile (LV-OOA)), and various particle- and gas-phase species, and ions.

r	HOA	COA	POA (HOA+ COA)	SV-OOA	LV-OOA	OOA (SV-OOA+ LV-OOA)
Nitrate	0.28	0.13	0.23	0.21	0.02	0.11
Sulfate	0.05	-0.05	0.00	-0.06	-0.03	-0.04
Ammonium	0.19	0.04	0.12	0.07	0.00	0.03
Chloride	0.47	0.13	0.32	0.05	-0.10	-0.05
K (AMS)	0.50	**0.68**	**0.70**	**0.73**	0.55	**0.70**
Primary pollutants						
BC	0.54	0.38	0.52	0.42	0.22	0.34
CO	0.36	0.30	0.38	0.23	0.03	0.12
NO_2	0.41	0.57	0.58	0.27	0.13	0.21
AMS tracer ions (*m/z* value)						
CO_2^+ (44)	0.22	0.31	0.31	0.61	**0.78**	**0.80**
$C_2H_5N^+$ (43)	0.10	0.18	0.17	0.64	0.58	0.68
$C_2H_4O_2^+$ (60)	0.39	0.62	0.60	**0.67**	**0.75**	**0.81**
$C_3H_5O_2^+$ (73)	0.35	0.61	0.58	**0.66**	**0.81**	**0.85**
$C_3H_3O^+$ (55)	0.39	**0.75**	**0.69**	**0.73**	**0.67**	**0.78**
$C_3H_5O^+$ (57)	0.37	0.61	0.59	**0.79**	**0.75**	**0.87**
$C_3H_7^+$ (43)	**0.87**	**0.80**	**0.97**	0.43	0.17	0.31
$C_3H_7N^+$ (57)	0	0.06	0.04	0.26	0.33	0.34
$C_4H_7^+$ (55)	**0.85**	**0.78**	**0.98**	0.52	0.24	0.40
$C_4H_9^+$ (43)	**0.81**	**0.84**	**0.96**	0.42	0.00	0.24
$C_5H_{11}^+$ (57)	**0.96**	0.60	**0.89**	0.28	0.04	0.15
$C_5H_8O^+$ (84)	0.46	**0.89**	**0.82**	0.60	0.41	0.55
$C_6H_{10}O^+$ (98)	0.46	**0.96**	**0.87**	0.38	0.20	0.31
$C_7H_{12}O^+$ (112)	0.40	**0.70**	**0.66**	0.44	0.30	0.41
$C_9H_7^+$ (115)	0.54	**0.71**	**0.74**	**0.72**	0.59	**0.73**
CHN^+ (27)	0.23	0.25	0.28	0.37	0.47	0.49
CN^+ (26)	0.15	0.29	0.26	0.11	0.08	0.11
$CH_2SO_2^+$ (77)	0.20	0.09	0.16	0.06	0.04	0.05
$CH_3SO_2^+$ (78)	0.21	0.09	0.17	0.05	0.03	0.04

BC, black carbon; AMS, aerosol mass spectrometer; PAH, polycyclic aromatic hydrocarbons
Value that are r > 0.7 are boldfaced

Atmos. Chem. Phys. Discuss., https://doi.org/10.5194/acp-2017-947
Manuscript under review for journal Atmos. Chem. Phys.
Discussion started: 8 November 2017

Figures

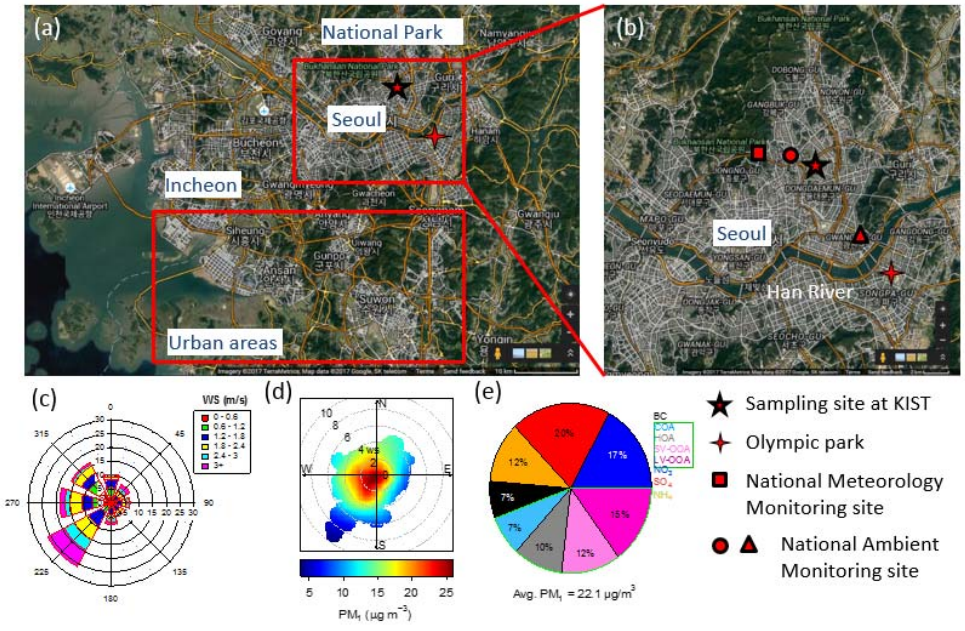

Figure 1. (a) The map of SMA and surrounded by other nearby cities including Incheon where industrial facilities are located (west and south) and agricultural and biogenic areas (east and south) and Bukhansan national park (north). Also shown the other supersite located at Olympic park; **(b)** The location of sampling site in Seoul which is at the north-east of the city center and north of Han river **(c)** Wind rose plot for the entire study period; **(d)** Bivariate polar plots of PM_1 (non-refractory-PM_1 plus black carbon (BC)) concentrations (in $\mu g/m^3$); **(e)** Average compositional pie chart of PM_1 species and each of the OA factors over the whole campaign. The green outline indicates the fraction of total OA.

Atmos. Chem. Phys. Discuss., https://doi.org/10.5194/acp-2017-947
Manuscript under review for journal Atmos. Chem. Phys.
Discussion started: 8 November 2017

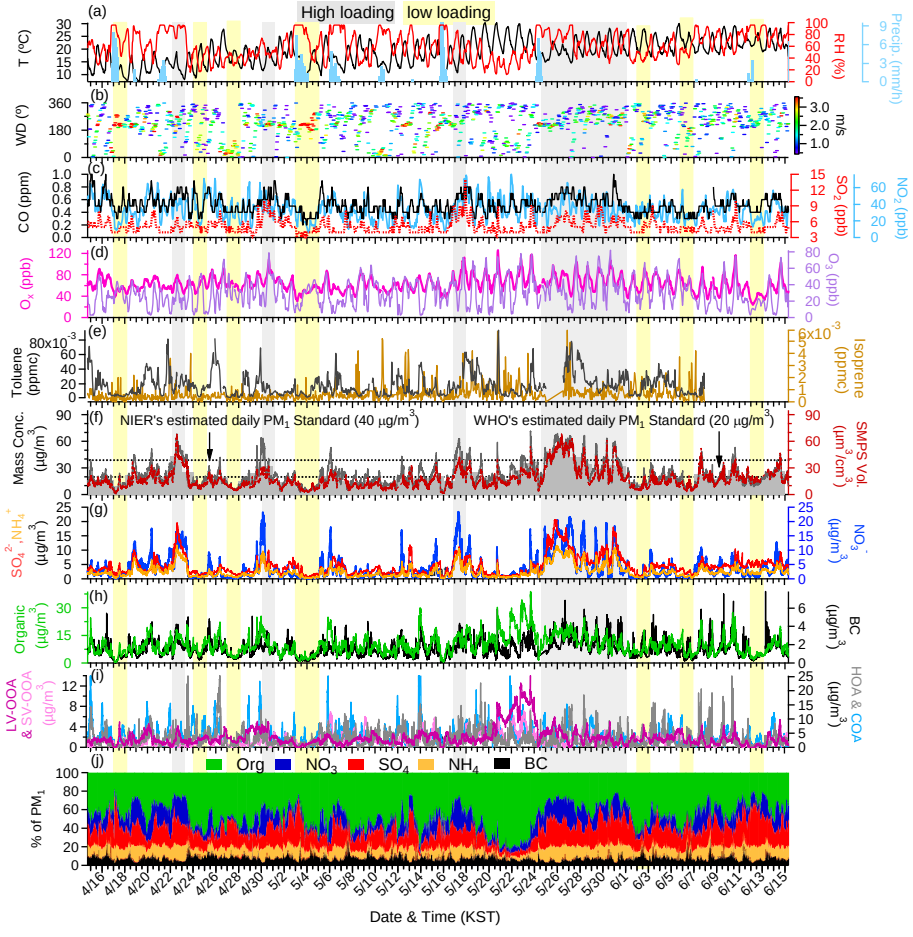

Figure 2. Overview of the temporal variations of submicron aerosols at the Korea Institute of Science and Technology (KIST) in SMA from April 14, 2016 to June 15, 2016: **(a)** Time series of ambient air temperature (T), relative humidity (RH), and precipitation (Precip.); **(b)** Time series of wind direction (WD), with colors showing different wind speeds (WS); **(c)** Time series of CO,SO_2, and NO_2; **(d)** Time series of O_x (NO_2 + O_3) and O_3; **(e)** Time series of toluene and isoprene; **(f)** Time series of total particulate matter (PM_1), scanning mobility particle sizer (SMPS) volume concentrations and also shown are the 24 h averaged PM_1+BC with bars. Estimated NIER's and WHO's daily PM_1 standards (40 μg/m^3 and 20 μg/m^3, respectively) are also shown with dashed line for the comparisons; **(g)** Time series of the nitrate (NO_3^-), sulfate (SO_4^{2-}) and ammonium (NH_4^+) aerosols; **(h)** Time series of the organic (Org.) and BC aerosols; **(i)** Time series of each factor derived from the positive matrix factorization (PMF) analysis; **(j)**Time series of the mass fractional contribution of organic aerosols (Org.), nitrate (NO_3^-), sulfate (SO_4^{2-}), ammonium (NH_4^+), and BC to total PM_1

Atmos. Chem. Phys. Discuss., https://doi.org/10.5194/acp-2017-947
Manuscript under review for journal Atmos. Chem. Phys.
Discussion started: 8 November 2017

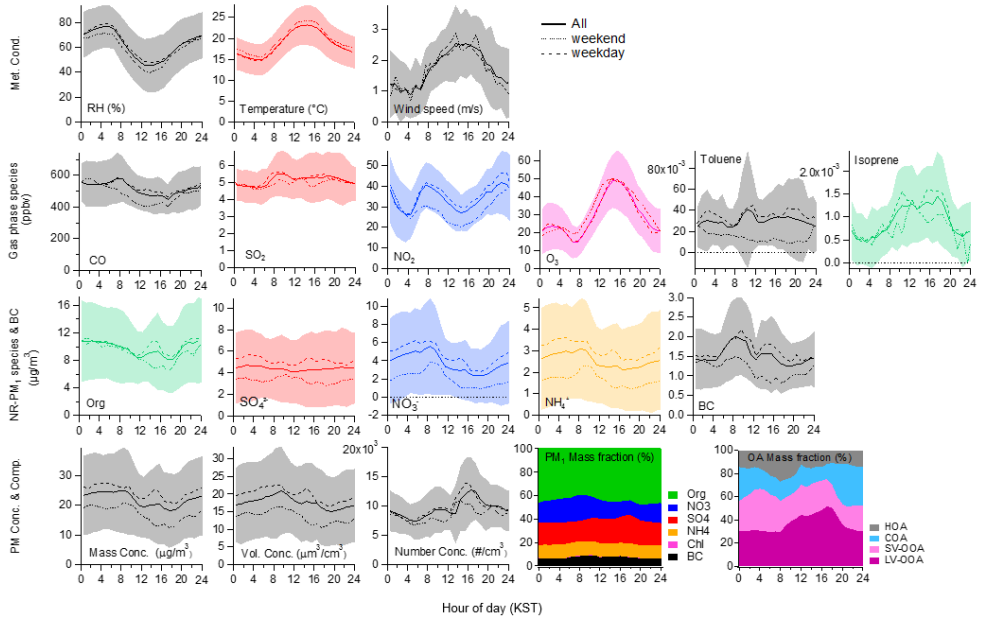

Figure 3. One-hour averaged diurnal profiles for the various meteorological parameters (top row), gas phase species (second row from the top), PM_1 species (third row) and PM mass concentration, volume concentration, number concentration, PM_1 composition, and organic aerosol composition.

Atmos. Chem. Phys. Discuss., https://doi.org/10.5194/acp-2017-947
Manuscript under review for journal Atmos. Chem. Phys.
Discussion started: 8 November 2017

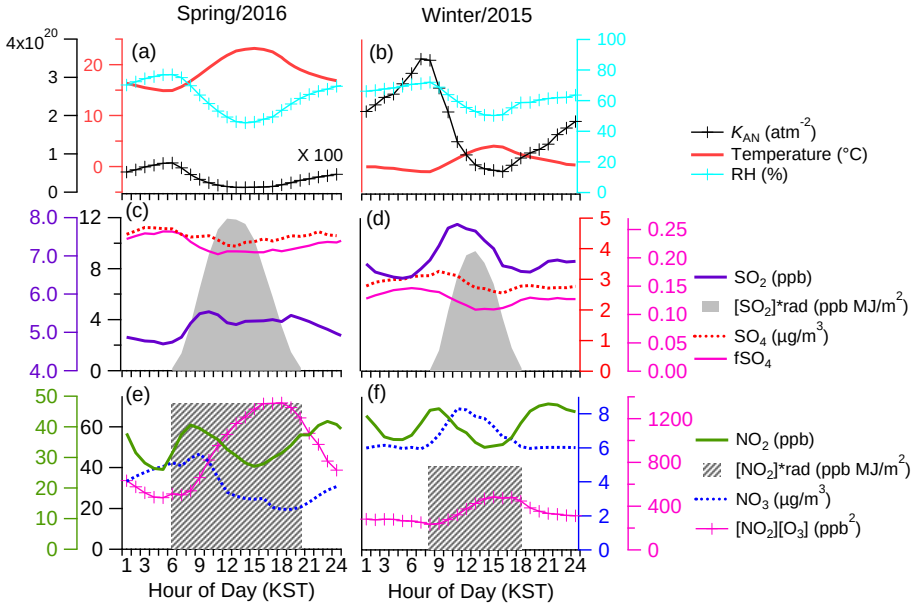

Figure 4. One-hour averaged diurnal profiles for sulfate, nitrate and various parameters and proxies for formation pathways in 2015 winter and 2016 spring; Temperature, relative humidity and K_{AN} as the equilibrium constant for gas-to-particle partitioning for ammonium nitrate in **(a)** 2016 and **(b)** 2015. The equilibrium constant k_{AN} can be calculated as:

$$k_{AN} = k(298)exp\left\{a\left(\frac{298}{T} - 1\right) + b\left[1 + \ln\left(\frac{298}{T}\right) - \frac{298}{T}\right]\right\}$$

where T is the ambient temperature in Kelvin, $k(298)$ = 3.36 x 10^{16} (atm^{-2}), a = 75.11, and b = -13.5 (Seinfeld and Pandis, 2006). The one-hour averaged diurnal profiles of SO_2, SO_4, fSO$_4$ and [SO_2] times solar radiation as a proxy for daytime H_2SO_4 formation in **(c)** spring, 2016 **(d)** winter, 2015; the one-hour averaged diurnal profiles of NO_2, NO_3, [NO_2][O_3] as a proxy for nighttime formation of HNO_3 and subsequently particulate nitrate, and [NO_2] times solar radiation as a proxy for daytime HNO_3 formation in **(e)** spring, 2016 **(f)** winter, 2015.

Atmos. Chem. Phys. Discuss., https://doi.org/10.5194/acp-2017-947
Manuscript under review for journal Atmos. Chem. Phys.
Discussion started: 8 November 2017

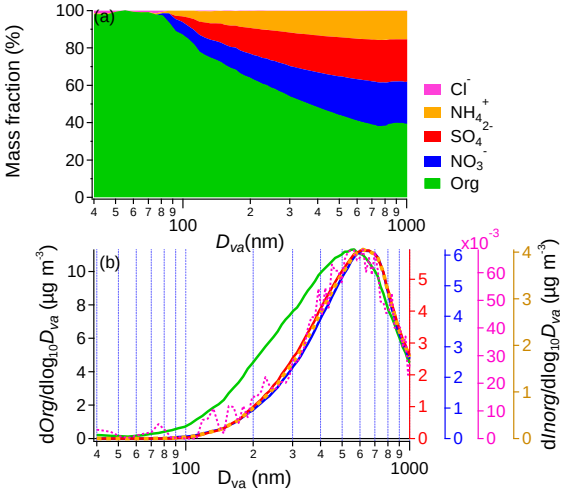

Figure 5. (a) Averaged mass fractional contributions of each NR-PM_1 species to the total NR-PM_1 mass as a function of size; **(b)** Campaign-averaged size distributions for individual NR-PM_1 species

Atmos. Chem. Phys. Discuss., https://doi.org/10.5194/acp-2017-947
Manuscript under review for journal Atmos. Chem. Phys.
Discussion started: 8 November 2017

Atmospheric Chemistry and Physics Discussions

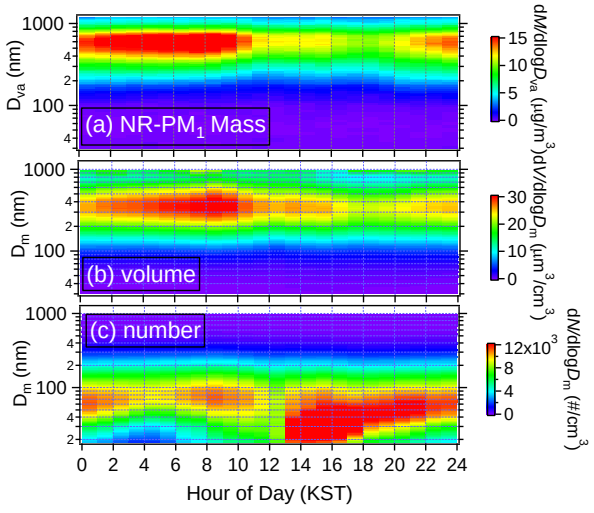

Figure 6. (a) Diurnal variations of the size distribution of NR-PM$_1$ mass from the AMS (in vacuum aerodynamic diameter, D_{va}); **(b)** volume from the SMPS (in mobility diameter, D_m**)** and **(c)** number concentrations from the SMPS

Atmos. Chem. Phys. Discuss., https://doi.org/10.5194/acp-2017-947
Manuscript under review for journal Atmos. Chem. Phys.
Discussion started: 8 November 2017

Atmospheric Chemistry and Physics Discussions

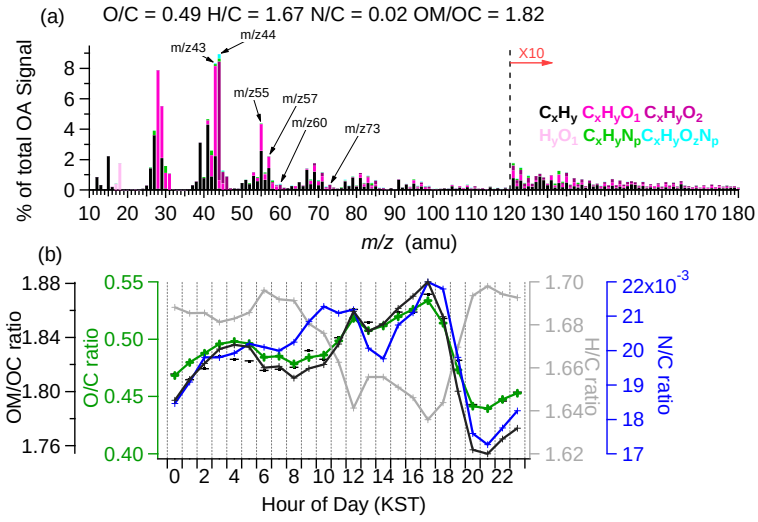

Average PM_1 composition (22.1 µg/m^3)		Average OA ratios		Average OA spectral composition	
Org	44%	O/C	0.49	$C_xH_y^+$	47 %
Sulfate	17%	H/C	1.67	$H_yO_1^+$	2.4 %
Nitrate	20%	N/C	0.02	$C_xH_yO_1^+$	31%
Ammonium	12%	S/C	0.002	$C_xH_yO_2^+$	14 %
Chloride	0%	OM/OC	1.82	$C_xH_yN_p^+$	3.3%
BC	7%			$C_xH_yN_pO_z^+$	2.3%

Figure 7. (a) Average high-resolution mass spectrum of OA colored by the different ion families. The average elemental ratios for the OA fraction are described; **(b)** Average diurnal profiles of the organic matter to organic carbon (OM/OC), oxygen to carbon (O/C), hydrogen to carbon (H/C), nitrogen to carbon (N/C), where the O/C, H/C and OM/OC elemental ratios were determined using the updated method (Canagaratna et al., 2015).Table shown is the Overview of the average PM_1 and OA compositions in SMA during KORUS-AQ

Atmos. Chem. Phys. Discuss., https://doi.org/10.5194/acp-2017-947
Manuscript under review for journal Atmos. Chem. Phys.
Discussion started: 8 November 2017

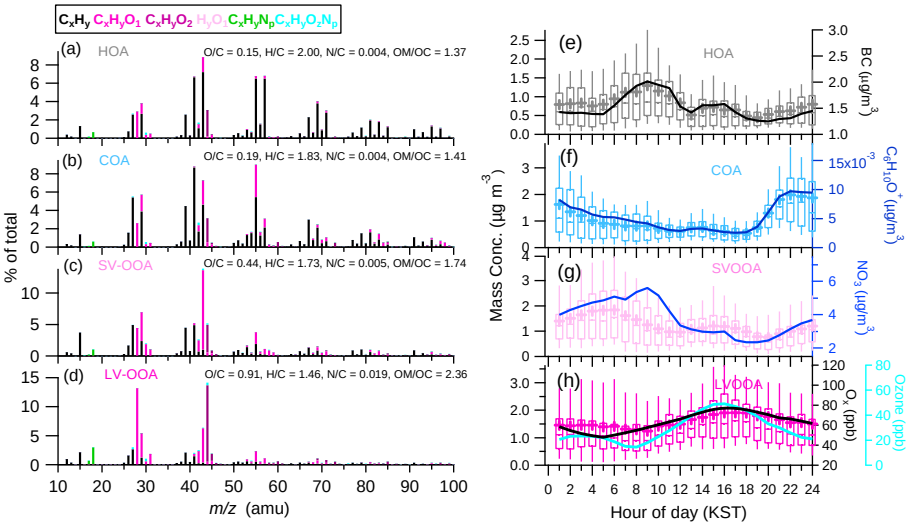

Figure 8. Overview of the results from PMF analysis including high-resolution mass spectra of the **(a)** Hydrocarbon-like organic aerosol (HOA), **(b)** Cooking OA (COA), **(c)** Semi volatile oxygenated OA (SV-OOA), and **(d)** Low volatility oxygenated OA (LV-OOA) colored by different ion families; **(e-h)** Average diurnal profiles of each of the OA factors (the 90th and 10th percentiles are denoted by the whiskers above and below the boxes, the 75th and 25th percentiles are denoted by the top and bottom of the boxes, the median values are denoted by the horizontal line within the box, and the mean values are denoted by the colored markers) with various tracer species.

Atmos. Chem. Phys. Discuss., https://doi.org/10.5194/acp-2017-947
Manuscript under review for journal Atmos. Chem. Phys.
Discussion started: 8 November 2017

Atmospheric Chemistry and Physics Discussions

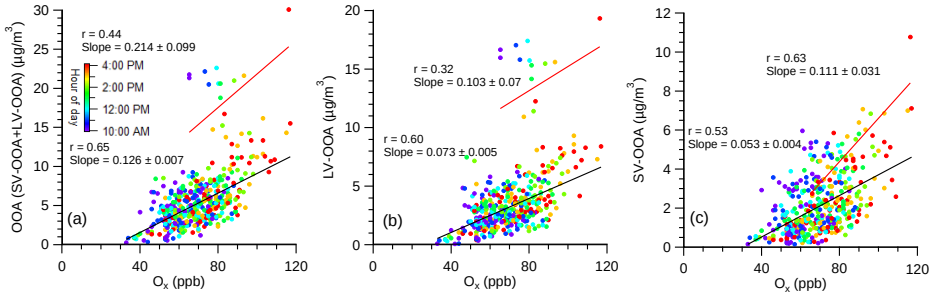

Figure 9. Scatter plots of **(a)** OOA; **(b)** LV-OOA; **(c)** SV-OOA vs O_x during daytime (10:00 - 16:00) in spring 2015. Note that the fitting for the organic dominant period (5/20, 17:00 - 5/24, 0:00) are colored by red and for the rest of periods are colored by black.

Atmos. Chem. Phys. Discuss., https://doi.org/10.5194/acp-2017-947
Manuscript under review for journal Atmos. Chem. Phys.
Discussion started: 8 November 2017

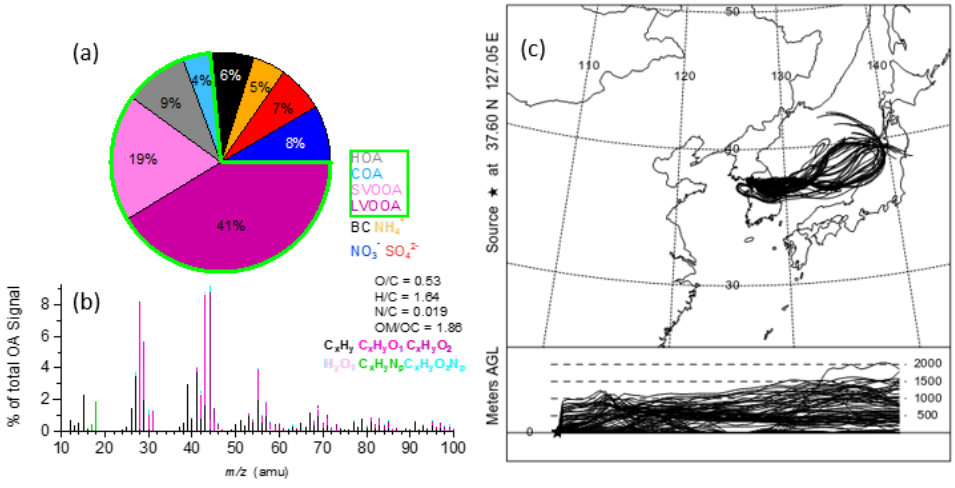

Figure 10. (a) Average compositional pie chart of PM_1 species (non-refractory-PM_1 plus black carbon (BC)) and each of the OA factors over an organic dominant period (5/20 17:00 - 5/24 0:00). The green outline indicates the fraction of total OA; and **(b)** Average high-resolution mass spectrum of OA colored by the different ion families. The average elemental ratios for the OA fraction are described (a); **(c)** Every hour back trajectories of air masses arriving at KIST during organic dominant period (5/20 17:00 - 5/24 0:00).

Atmos. Chem. Phys. Discuss., https://doi.org/10.5194/acp-2017-947
Manuscript under review for journal Atmos. Chem. Phys.
Discussion started: 8 November 2017

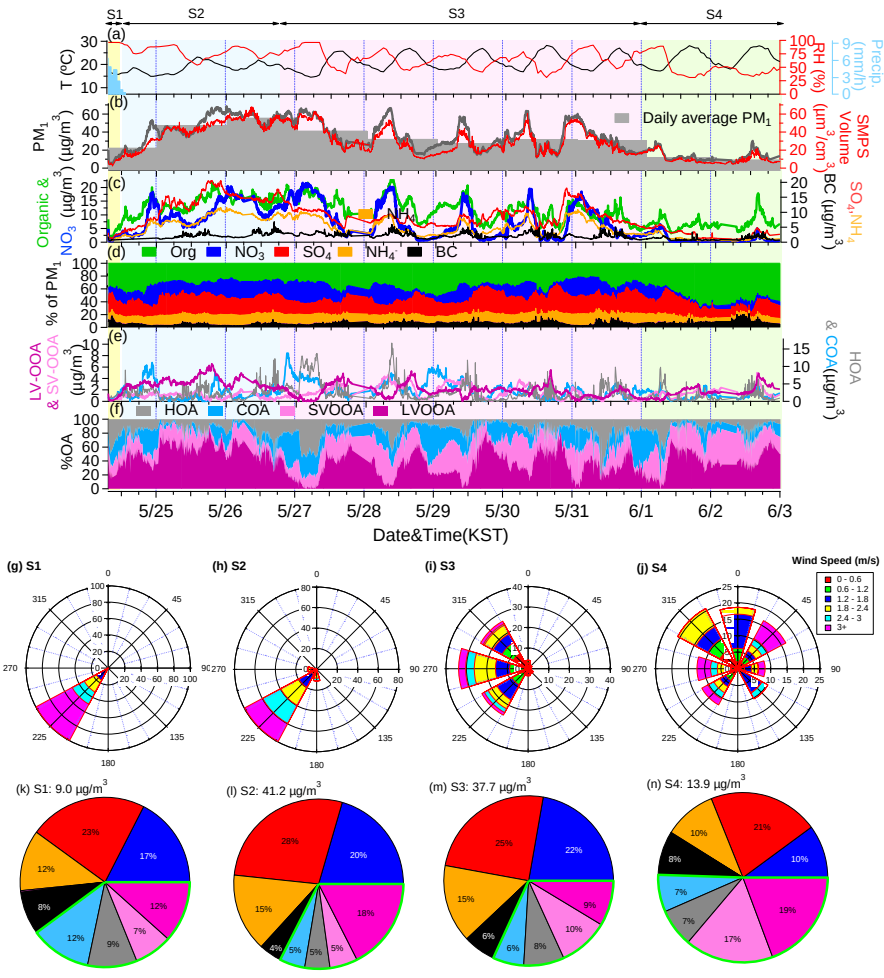

Figure 11. (a) Time series of ambient air temperature (T), relative humidity (RH), and precipitation (Precip.); **(b)** Time series of total particulate matter (PM_1), scanning mobility particle sizer (SMPS) volume concentrations, and the 24 h averaged PM_1+BC with bars; **(c)** Time series of the organic (Org.), nitrate (NO_3^-), sulfate (SO_4^{2-}), ammonium (NH_4^+) and BC aerosols; **(d)** Time series of the mass fractional contribution of organic aerosols (Org.), nitrate (NO_3^-), sulfate (SO_4^{2-}), ammonium (NH_4^+), and BC to total PM_1 concentration; **(e)** Time series of each factor derived from the positive matrix factorization (PMF) analysis; **(f)** Time series of mass fractional contribution of OA factors to OA; **(g-j)**Wind rose plots, colored by wind speed and; **(k-n)** Fractional contributions of each species to the total PM_1 (non-refractory-PM_1 plus BC) mass for each stage in haze life.